Imperial College London

Department Of Theoretical Physics

Curvature And Topology On Causal Sets

Bernhard Schmitzer

September 14, 2010

Supervised By Fay Dowker

Submitted in partial fulfilment of the requirements for the

degree of Master of Science of Imperial College London

Abstract

This thesis focusses on the relation between causal sets and Lorentzian manifolds. Especially the effects of curvature and non-trivial topology are investigated. It is described how causal sets can be stochastically created from a given manifold via the sprinkling process. In the course of establishing a causet equivalent for the language of partial differential equations both the retarded propagator of the Klein-Gordon equation and a discrete version of the d'Alembert operator are examined. A more generalized propagator is proposed that can handle the effects of non-trivial topology by using the newly introduced homotopy matrix. The interplay of the propagator and spacetime curvature is discussed in two and four dimensions. An algorithm to approximately recover the homotopy matrix from the causal structure is given. The discrete d'Alembertian is used to make the scalar curvature of causal sets visible in two dimensional de Sitter space. A hierarchy of different physical length scales and their mutual interplay is numerically analysed. A proposed candidate for a two dimensional causal set action is investigated both analytically and numerically for hints of topological invariance, fluctuations and the reaction to the presence of curvature.

Acknowledgements

The author would like to thank the Imperial College High Performance Computing Service for the provided computation resources and the creators of gnuplot for creating such a helpful piece of software.

Noel Hustler, Lisa Glaser and Dionigi Benincasa are thanked for fruitful discussions and some other persons deserve extra credit for a lot of listening skills and patience.

I am particularly grateful to Fay Dowker for being a very committed, supportive and wise supervisor.

(This thesis comes with a CD-ROM)

Contents

Chapter 1

Introduction

1.1 Fundamental Physics And Discrete Spacetime

Today the established theories to describe space, time and matter are general relativity and quantum field theory. We are aware that they do not give a complete description of nature yet. Especially the unification of both appears to be a hard problem and a lot of effort is made to find a more general *theory of everything*. The backbone of general relativity, quantum field theory and also of many approaches that seek to supersede them is the notion of continuous spacetime which is described by Lorentzian manifolds.

However we suspect that something must change fundamentally if we "zoom in" to very small length scales. Clues for that are singularities that appear in general relativity and the fact that we must cut off momentum integrals in quantum electrodynamics. The assumption that electrons behave the same way on arbitrary small length scales leads to diverging amplitudes.

There is a wide variety of proposals what that fundamental change might be: Additional internal particle structures or hidden dimensions are potential solutions. Others believe that the fabric of spacetime itself will start to look different and on small scales can no longer be described by smooth manifolds.

Causal sets are an alternative approach to describe spacetime. In causal set theory spacetime is no longer assumed to be continuous but to be constituted of a discrete set of elements. The whole causal, topological and metric structure, all the concepts that we know from continuous manifolds and that we know work very well on bigger length scales, all this is conjectured to be encoded in nothing but a partial order of the set elements. Not every causal set approximates a manifold. However the "Hauptvermutung" of causal set theory is that if a set does start to look like a manifold on large scales then this manifold is "approximately unique" [1].

The following thesis will discuss the relation of causal sets and smooth manifolds and how information about curvature and topology is encoded in the partial ordering.

1.2 Definition Of A Causal Set

A causal set or *causet* is a partially ordered locally finite set. That means it is a set $\mathcal{C}$ and a partial order relation $\prec$ for elements of $\mathcal{C}$ that satisfy the following conditions:

- $\prec$ is transitive: $(x \prec y) \wedge (y \prec z) \Rightarrow x \prec z$.
- $x \prec x$ is *not* true.
- $\mathcal{C}$ is locally finite: $n(x,y) = |\{z \in \mathcal{C} \mid x \prec z \prec y\}|$ is finite $\forall\ x, y \in \mathcal{C}$ where $|\cdot|$ denotes set cardinality.

For $x \prec y$ we can also write $y \succ x$. For $(x \prec y) \vee (x = y)$ we write $x \preceq y$. Hence $x \prec y \Leftrightarrow (x \preceq y) \wedge (x \neq y)$. If $x \prec y$ and $n(x,y) = 0$ we write $x \prec\!\!\!* \, y$ and say that y is linked to x.

An ordered subset $c = (z_1, z_2, \ldots, z_{n+1}) \subset \mathcal{C}$ with $z_1 \prec z_2 \prec \ldots \prec z_{n+1}$ will be referred to as n-chain with n jumps between successive elements. An ordered subset $p = (z_1, z_2, \ldots, z_{n+1})$ with $z_1 \prec\!\!* \, z_2 \prec\!\!* \, \ldots \prec\!\!* \, z_{n+1}$ is called n-path with n jumps. Every n-path is a n-chain. An element $x \in s \subset \mathcal{C}$ is called *minimal* in s if $\nexists\ y \in s$ such that $y \prec x$ and *maximal* if $\nexists\ y \in s$ such that $x \prec y$.

The information about all relations $\prec$ between the set elements is equivalent to the knowledge of all relations $\prec\!\!\!*$:

$$\begin{aligned} x \prec\!\!\!* \, y \quad &\Leftrightarrow \quad (x \prec y) \wedge (n(x,y) = 0), \text{ all other relations follow from transitivity} \\ x \prec y \quad &\Leftrightarrow \quad \exists \text{ a } n\text{-path } p = (x, z_1, \ldots, z_{n-1}, y) \subset \mathcal{C} \text{ for some } n \geq 1 \end{aligned}$$

Consider a causal set $\mathcal{C}$ and label its elements in some order such that any element x_i can be referred to by some index i. Then we can define two *adjacency matrices* A_C and A_R with

$$(A_C)_{ij} = \begin{cases} 1 & \text{if } x_i \prec x_j \\ 0 & \text{else} \end{cases} \qquad\qquad (A_R)_{ij} = \begin{cases} 1 & \text{if } x_i \prec\!\!\!* \, x_j \\ 0 & \text{else} \end{cases} . \tag{1.1}$$

These matrices are called the *causal matrix* and the *link matrix*.

Discrete subsets of points of Lorentzian manifolds can be interpreted as causets where the order relation is induced by causal relations on the manifold: We write $x \prec y$ if and only if x strictly precedes y on the manifold, i.e. if $y \in J^+(x) \ \wedge x \neq y$.

Throughout literature there are slight differences in the definitions of causal sets. In the end they are all equivalent and describe the same concept. However the reader must be careful not to mix things up.

Chapter 2

Sprinklings

2.1 The Correspondence Between Causal Sets And Lorentzian Manifolds

Causal sets are an attempt to replace the concept of smooth Lorentzian manifolds by a discrete graph of causally related nodes. It has been shown that Lorentzian manifolds satisfying a causality condition known as *past and future distinguishing* are fully characterized by their causal structure and a notion of measuring volumes [2, 3, 4]. So a causal set must try to at least approximately encode this information in order to be able to replace the manifold.

In a causet the causal structure of the elements is represented by the partial order relation on the set. A prescription of measuring volume is given by counting the number of elements in a given subset and multiplying this by an elementary Planckian volume that each single element "takes up". These are simple and precise definitions of causal relationship and volume. Yet it is hard to define a clear understanding as to when a causal set can be regarded as approximation of a given smooth Lorentzian manifold or the other way round depending on your point of view.

An attempt to tackle this issue is the concept of sprinkling. A sprinkling is a stochastic process to generate a causal set from a Lorentzian manifold. This serves two purposes:

On one hand it helps establishing a relation between a causal set $\mathcal{C}$ and a manifold $\mathcal{M}$ by saying $\mathcal{C}$ and $\mathcal{M}$ describe approximately the same universe if $\mathcal{C}$ is likely to be produced by a sprinkling into $\mathcal{M}$.

On the other hand it is the only way to generate causal sets at the moment that are definitely "manifold like" whatever notion of comparison one might use. Attempts to create such causal sets "from scratch", i.e. from a fundamental dynamical law, are to this date not very successful [5, 6].

2.2 The Sprinkling Process

The sprinkling process creates a causal set $\mathcal{C}$ from a (patch of a) Lorentzian manifold $\mathcal{M}$ in a stochastic way by randomly picking points from $\mathcal{M}$ with a constant finite density ρ of points per spacetime volume of $\mathcal{M}$. The points form a partially ordered set with the order relation induced by the causal relation on $\mathcal{M}$.

Picking the points with a constant density means one expects $\rho \cdot V(\Omega)$ points to be taken from any region $\Omega \subset \mathcal{M}$, i.e. a single point is interpreted to "take up" the volume of about $1/\rho$. Here $V(\Omega)$ denotes the spacetime volume of the region Ω. Thus the volume measure on $\mathcal{C}$ on average agrees with the one on $\mathcal{M}$: The part of the causal set that corresponds to a region Ω will on average contain $\rho \cdot V(\Omega)$ elements with a volume of $1/\rho$ per element thus yielding $V(\Omega)$ as the expected volume.

Picking the points by chance also ensures that there will be no preferred or distinguished directions on the manifold like choosing points from a grid would imply. This conserves any symmetries of the spacetime.[1] The random picking therefore ensures the compatibility of the causal set and the manifold description.

If the volume of $\mathcal{M}$ is infinite so will be the number of points in $\mathcal{C}$. However $\mathcal{C}$ will remain locally finite meaning that the cardinality of any causal interval

$$n(x, y) = |\{z \in \mathcal{C} | x \prec z \prec y\}| \quad \forall \quad x, y \in \mathcal{C}$$

will be finite as the volume $V(x, y)$ of the causal interval between the points x and y on $\mathcal{M}$ will be finite.

For upcoming calculations it is essential to know the probability distribution $\mathrm{P}(n(\Omega) = n)$ describing how likely it is that a sprinkling into $\mathcal{M}$ will pick n points from the region $\Omega \subset \mathcal{M}$. As described for any region Ω the expected number of elements will be $\langle n(\Omega) \rangle = \rho \cdot V(\Omega)$. Now consider a very small region with a volume $V(\Omega) \ll \rho^{-1}$. It will most likely be empty (in the sense that no point from it will be picked for the sprinkling) and if it does indeed contain points it will most likely be only a single one. Thus the number of expected elements can be written as

$$\langle n(\Omega) \rangle = \rho \cdot V(\Omega) \approx 0 \cdot \mathrm{P}(n(\Omega) = 0) + 1 \cdot \mathrm{P}(n(\Omega) = 1) \tag{2.1}$$

for $V(\Omega) \ll \rho^{-1}$ where we can neglect contributions of $n(\Omega) > 1$. So one can conclude

$$\begin{aligned} \mathrm{P}(n(\Omega) = 0) &\approx 1 - \rho \cdot V(\Omega) \\ \mathrm{P}(n(\Omega) = 1) &\approx \rho \cdot V(\Omega) \\ \mathrm{P}(n(\Omega) > 1) &\approx 0. \end{aligned} \tag{2.2}$$

[1] Poincaré symmetry is a continuum specific way of stating that there is no preferred frame. So naturally on a causet there is no translation symmetry but still there is no preferred frame. So the symmetry is preserved in a more general sense.

Using this we can compute $\mathrm{P}(n(\Omega) = n)$ for finite volumes: Split up the region into k parts of equal volume $V(\Omega)/k$ then for large enough k all cells contain either none or one point with the respective probabilities. So we only need to multiply the uncorrelated partial probabilities for the individual cells with the correct combinatorial factor:

$$\begin{aligned}
\mathrm{P}(n(\Omega) = n) &= \lim_{k\to\infty} \binom{k}{n} (1 - \rho \cdot V(\Omega)/k)^{(k-n)} (\rho \cdot V(\Omega)/k)^n \\
&= \lim_{k\to\infty} \underbrace{\frac{k!}{(k-n)!\, k^n}}_{\to 1} \underbrace{\left(1 - \frac{\rho \cdot V(\Omega)}{k}\right)^{-n}}_{\to 1} \underbrace{\left(1 - \frac{\rho \cdot V(\Omega)}{k}\right)^{k}}_{\to \exp(-\rho \cdot V(\Omega))} \frac{(\rho \cdot V(\Omega))^n}{n!} \\
&= \exp(-\rho \cdot V(\Omega)) \frac{(\rho \cdot V(\Omega))^n}{n!} \qquad (2.3)
\end{aligned}$$

This is a Poisson distribution with a mean of $\rho \cdot V(\Omega)$ and a standard deviation of $\sqrt{\rho \cdot V(\Omega)}$. So for very large ρ not only does the average of the volume measurement on $\mathcal{C}$ agree with the one on $\mathcal{M}$ but also the fluctuations become smaller with $\sqrt{V(\Omega)/\rho}$.

Note that the elements of a causal set generated by a sprinkling no longer contain any information about their original position on the manifold. We may however sometimes remember that information in order to compare the causet results to the continuum. Yet the only information that may be used within causal set calculations themselves is the causal relation of points.

2.3 Creating A Sprinkling

As pointed out the sprinkling process is at the moment the only reliable way to create causal sets that correspond to spacetimes that we usually describe with smooth Lorentzian manifolds. The sprinkling process is therefore an indispensable tool in the investigation of the properties of such sets. Especially for computer simulations we need to explicitly create causal sets from manifolds. Therefore it shall be described how this can be achieved.

On a computer one usually can draw on a generator for pseudo random numbers that are evenly distributed in the interval $[0, 1]$ and thus by multiple calls of this generator one can create evenly distributed elements in $[0, 1]^d \subset \mathbb{R}^d$. To create sprinklings into a region Ω on a d-dimensional manifold $\mathcal{M}$ one must define a suitable map $f : [0, 1]^d \to \Omega$, $x \mapsto z$ which distributes the points with homogeneous density. Therefore for any region $A \subset [0, 1]^d$ and its image $f(A) \subset \Omega$ we must have:

$$V(\Omega) \int_A d^d x = \int_{f(A)} d^d z \sqrt{-g}$$

Here g is the metric determinant on $\mathcal{M}$ and the factor $V(\Omega)$ on the left-hand side is required to scale up the volume of the (hyper-)cube with unit edge length to the volume of Ω. Here f can be interpreted as a coordinate transformation and thus we see that the Jacobian $J = |\det(\partial z/\partial x)|$ of this transformation must satisfy

$$J = V(\Omega)/\sqrt{-g}. \qquad (2.4)$$

f must be both a surjective and an injective map between $[0,1]^d$ and Ω apart from subsets of measure zero.[2]

Having found such a map f the actual sprinkling can be performed like this: First one determines the overall number of points one wants to sprinkle. One can do this by either fixing this number or by fixing the density and then picking the total number of elements at random according to the Poisson distribution. Then one picks the desired number of points from the hypercube $[0,1]^d$, which can be done easily on a computer, maps them to Ω and deduces their causal relations.

Without further guidelines however it seems hard to find a map that satisfies the constraint Eq. (2.4). But usually there is a straightforward way to construct a suitable map which should become clear when looking at the following examples with increasing complexity.

2.4 Finding The Sprinkling Map

2.4.1 Minkowski 2d: $\mathbb{M}^2$

We consider sprinklings into a causal interval. Due to Poincaré symmetry we can always choose the coordinates of the start- and endpoint to be $(0,0)$ and $(T,0)$ in the usual (t,x) coordinates with the flat metric $g_{\mu\nu} = \eta_{\mu\nu}$ with $\sqrt{-g} = 1$. For a causal interval the most convenient coordinate system are lightcone coordinates

$$\begin{aligned} u &= \tfrac{1}{\sqrt{2}}(t+x) \\ v &= \tfrac{1}{\sqrt{2}}(t-x). \end{aligned} \tag{2.5}$$

The Jacobian determinant of this transformation is 1 so $\sqrt{-g} = 1$ in (u,v)-coordinates. The causal interval is described by $(u,v) \in [0,a]^2$ with $a = T/\sqrt{2}$ and its volume is $V = a^2 = T^2/2$. We must now find a map

$$f : [0,1]^2 \to [0,a]^2,\ x = (x_1, x_2) \mapsto z = (u,v)$$

with $J = |\det(\partial z/\partial x)| = a^2$.

As the metric determinant is constant in the (u,v)-coordinates we can tell that any point (u,v) in the interval is equally likely. So one only needs to construct a suitable map that scales the two dimensional square $[0,1]^2$ to $[0,a]^2$ which can be done easily:

$$f : \begin{pmatrix} x_1 \\ x_2 \end{pmatrix} \mapsto \begin{pmatrix} u = a \cdot x_1 \\ v = a \cdot x_2 \end{pmatrix}$$

One can immediately see that the Jacobian determinant of this transformation is indeed a^2.

[2] f can also be chosen not to be injective, then $\sum_i J(x_i) = V(\Omega)/\sqrt{-g(z)}$ for all x_i s.t. $f(x_i) = z$. We choose f to be injective for simplicity.

2.4.2 Minkowski 3d: $\mathbb{M}^3$

Consider now a causal interval on $\mathbb{M}^3$. Again one can use Poincaré symmetry and choose the points confining the interval to be $(0,0,0)$ and $(T,0,0)$ in Cartesian coordinates (t,x,y). The causal interval is

$$\left\{(t,x,y) \in [0,T] \times \mathbb{R}^2 \mid \sqrt{x^2+y^2} \leq \min\{t, T-t\}\right\}.$$

In dimensions higher than two the causal interval is no longer just a tilted square so we cannot simply use the lightcone coordinates again.

There are two major approaches to generate a sprinkling into this region: One could sprinkle points into the cube $[0,T] \times [-T/2, T/2]^2$ that contains the causal interval. This is an easy task. Then one throws away all points that are outside of the interval.

Let us instead use polar coordinates (τ, r, φ) this time:

$$\begin{aligned} t &= \tau \\ x &= r \cdot \cos(\varphi) \\ y &= r \cdot \sin(\varphi) \end{aligned} \tag{2.6}$$

The causal interval is described by

$$\Omega = \{(\tau, r, \varphi) \in [0,T] \times [0, \infty[\times [0, 2\pi] \mid r \leq \min\{\tau, T-\tau\}\}$$

and $\sqrt{-g} = r$ in these coordinates. The strategy to find a suitable sprinkling map $f : [0,1]^3 \to \Omega$, $(x_1, x_2, x_3) \mapsto (\tau, r, \varphi)$ will be to map layers of the cube $\{(x_1, x_2, x_3) \mid (x_2, x_3) \in [0,1]^2\}$ with constant x_1 to layers of the interval with constant τ such that $V(\Omega) \cdot x_1 = V(\Omega_\tau)$ where $\Omega_\tau = \{(\tau', r, \varphi) \in \Omega \mid \tau' \leq \tau\}$ denotes the part of the interval with $\tau' \leq \tau$. We define $f_1 : [0,1] \to [0,T]$, $x_1 \mapsto \tau$ to satisfy this. Consider the volume of Ω_τ:

$$\begin{aligned} V(\Omega_\tau) &= \int_{\Omega_\tau} d^3z \sqrt{-g} \\ V(\Omega_\tau \mid 0 \leq \tau \leq T/2) &= \int_0^\tau d\tau' \int_0^{\tau'} dr \int_0^{2\pi} d\varphi \; r \\ &= \frac{\pi}{3}\tau^3 \\ V(\Omega_\tau \mid T/2 \leq \tau \leq T) &= V(\Omega_T) - V(\Omega_{T-\tau}) \\ &= 2V(\Omega_{T/2}) - V(\Omega_{T-\tau}) \\ &= \frac{\pi}{3}\left(\frac{1}{4}T^3 - (T-\tau)^3\right) \end{aligned} \tag{2.7}$$

We can then conclude that f_1 has to satisfy

$$V(\Omega) \cdot x_1 = V\left(\Omega_\tau \mid \tau = f_1(x_1)\right). \tag{2.8}$$

This condition can be solved for $\tau = f_1(x_1)$ and one finds

$$\tau = \begin{cases} T \cdot \left(\frac{x_1}{4}\right)^{1/3} & \text{for} \quad 0 \leq x_1 \leq 1/2 \\ T \cdot \left(1 - \left(\frac{1-x_1}{4}\right)^{1/3}\right) & \text{for} \quad 1/2 \leq x_1 \leq 1 \end{cases}. \tag{2.9}$$

Now we proceed by finding a function that maps lines of the cube $\{(x_1, x_2, x_3) \mid x_3 \in [0,1]\}$ with constant x_1 and x_2 to subsets of Ω with constant $\tau = f_1(x_1)$ and constant $r = f_2(x_1, x_2)$ such that the two dimensional volume $V(D_{\tau,r})$ of the disc $D_{\tau,r} = \{(\tau, r', \varphi) \mid 0 < r' < r,\, \varphi \in [0, 2\pi]\}$ satisfies $V(D_{\tau,r}) = x_2 \cdot V(D_{\tau,r_{\max}})$ with $r_{\max} = \min\{\tau, T - \tau\}$. The two dimensional metric for the disc is formally obtained by pulling back the metric of $\mathbb{M}^3$ via the embedding of the disc into $\mathbb{M}^3$. The two dimensional metric is Riemannian (since we are on a spacelike surface) and its determinant gives $\sqrt{g} = r$. So naturally $V(D_{\tau,r}) = r^2\pi$ is the area of a regular Euclidean disc with radius r. One finds

$$\begin{aligned} V(D_{\tau,r} \,|\, \tau = f_1(x_1),\, r = f_2(x_1,x_2)) &= x_2 \cdot V(D_{\tau,r_{\max}} \,|\, \tau = f_1(x_1),\, r_{\max} = \min\{f_1(x_1), T - f_1(x_1)\}) \\ r^2\pi &= x_2 \cdot r_{\max}^2 \pi \\ r &= r_{\max} \cdot \sqrt{x_2}. \end{aligned} \tag{2.10}$$

Finally we need to take points from the line with constant x_1 and x_2 to the circles with constant τ and r. As all φ are equally likely this can be done by

$$\varphi = f_3(x_3) = 2\pi \cdot x_3. \tag{2.11}$$

Summarizing Eqns. (2.9,2.10,2.11) we find

$$\begin{array}{lll} 0 \le x_1 \le 1/2: & & 1/2 < x_1 \le 1: \\ \tau &= T\left(\frac{x_1}{4}\right)^{1/3} & \tau &= T\left(1 - \left(\frac{1-x_1}{4}\right)^{1/3}\right) \\ r &= \tau\, x_2^{1/2} & r &= (T-\tau)\, x_2^{1/2} \\ \varphi &= 2\pi \cdot x_3 & \varphi &= 2\pi \cdot x_3 \end{array} \tag{2.12}$$

and it can be verified that in both areas $|\det(\partial(\tau, r, \varphi)/\partial(x_1, x_2, x_3))| = V(\Omega)/r$ as required by Eq. (2.4).

After placing the points in the interval it will be necessary to compute their mutual causal relations. To this end it is probably most convenient to switch back to Cartesian coordinates which is readily done by using Eqns. (2.6).

The precise sprinkling into the interval seems like a very tedious task and one would be tempted to simply use the method with the cube that contains the interval briefly described above. However this way turns out to be a valuable exercise for sprinklings into curved spacetimes where successively finding the "sub maps" by integration is necessary.

2.4.3 Minkowski 4d: $\mathbb{M}^4$

Again we choose an interval that is bounded by $(T, 0, 0, 0)$ and $(0, 0, 0, 0)$ in Cartesian coordinates (t, x, y, z). And again one has the choice between embedding the interval into a hypercube, do the sprinkling into the cube and then remove unsuitable points or to find the more complicated map for

the interval itself analogous to the 3d case. A sketch of the derivation of this map follows: We will work in spherical coordinates

$$\begin{aligned} t &= \tau \\ x &= r\,\sin(\theta)\,\cos(\varphi) \\ y &= r\,\sin(\theta)\,\sin(\varphi) \\ z &= r\,\cos(\theta) \end{aligned} \tag{2.13}$$

in which the metric determinant yields $\sqrt{-g} = r^2\,\sin(\theta)$. The causal interval is described by

$$\Omega = \{(\tau, r, \theta, \varphi) \in [0,T] \times [0,\infty[\times [0,\pi] \times [0,2\pi] \mid r \leq \min\{\tau, T-\tau\}\}\,.$$

Like in three dimensions the first step will be finding a map $f_1 : x_1 \mapsto \tau$ that obeys

$$V(\Omega)\cdot x_1 = V(\Omega_\tau \mid \tau = f_1(x_1))$$

where $\Omega_\tau = \{(\tau', r, \theta, \varphi) \in \Omega \mid \tau' \leq \tau\}$. Integration yields

$$\begin{aligned} V(\Omega_\tau \,|\, 0 \leq \tau \leq T/2) &= \int_0^\tau d\tau' \int_0^{\tau'} dr \int_0^\pi d\theta \int_0^{2\pi} d\varphi\, r^2 \sin(\theta) = \frac{\pi}{3}\tau^4 \\ V(\Omega_\tau \,|\, T/2 \leq \tau \leq T) &= V(\Omega_T) - V(\Omega_{T-\tau}) \\ &= \frac{\pi}{3}\left(\frac{1}{8}T^4 - (T-\tau)^4\right). \end{aligned} \tag{2.14}$$

So we find

$$\tau = \begin{cases} T\cdot\left(\frac{x_1}{8}\right)^{1/4} & \text{for} \quad 0 \leq x_1 \leq 1/2 \\ T\cdot\left(1-\left(\frac{1-x_1}{8}\right)^{1/4}\right) & \text{for} \quad 1/2 \leq x_1 \leq 1 \end{cases}. \tag{2.15}$$

The next coordinate to be fixed is $r = f_2(x_1, x_2)$ via the condition

$$V(B_{\tau,r} \mid \tau = f_1(x_1),\, r = f_2(x_1,x_2)) = x_2 \cdot V(B_{\tau,r_{\max}} \mid \tau = f_1(x_1),\, r_{\max} = \min\{f_1(x_1), T - f_1(x_1)\})$$

where $B_{\tau,r} = \{(\tau, r', \theta, \varphi) \mid 0 \leq r' \leq r,\, \theta \in [0,\pi],\, \varphi \in [0,2\pi]\}$ is a three dimensional ball and $V(B_{\tau,r}) = \frac{4\pi}{3}r^3$ its three dimensional volume. This gives

$$r = r_{\max}\cdot x_2^{1/3}. \tag{2.16}$$

We proceed with $\theta = f_3(x_3)$ and the condition $V(S_\theta \mid \theta = f_3(x_3)) = x_3 \cdot V(S_\pi)$ with $S_\theta = \{(\theta', \varphi) \mid 0 \leq \theta' \leq \theta,\, \varphi \in [0,2\pi]\}$ from which one deduces

$$\begin{aligned} 2\pi(1-\cos(\theta)) &= x_3 \cdot 4\pi \\ \theta &= \arccos(1-2x_3). \end{aligned} \tag{2.17}$$

The map is completed by again using $\varphi = 2\pi\cdot x_4$ which together with Eqns. (2.15,2.16,2.17) gives:

$$\begin{array}{lll} 0 \leq x_1 \leq 1/2: & & 1/2 < x_1 \leq 1: \\ \tau &= T\left(\frac{x_1}{8}\right)^{1/4} & \tau &= T\left(1-\left(\frac{1-x_1}{8}\right)^{1/4}\right) \\ r &= \tau\, x_2^{1/3} & r &= (T-\tau)\, x_2^{1/3} \\ \theta &= \arccos(1-2x_3) & \theta &= \arccos(1-2x_3) \\ \varphi &= 2\pi\cdot x_4 & \varphi &= 2\pi\cdot x_4 \end{array} \tag{2.18}$$

Once again one can verify that the condition for the Jacobian of this map (Eq. (2.4)) is satisfied and once again it is probably a good idea to transform back to Cartesian coordinates in the end by using (2.13).

2.4.4 de Sitter space 2d

De Sitter space plays an important role as a toy model spacetime as it exhibits curvature, serves as a model for an expanding and shrinking universe and is yet simple enough to be treated more or less analytically due to its high degree of symmetry [7]. It is therefore a natural first choice to investigate the properties of causal sets in the presence of curvature.

In this thesis conformally flat coordinates $(t, r) \in]-\infty, 0[\times]-\infty, \infty[$ will be used with the metric $g_{\mu\nu} = (\alpha/t)^2 \eta_{\mu\nu}$ (see [7] for 4d, 2d can be done just analogously). We will consider sprinklings into a causal interval Ω between points $(t_0, 0)$, $(t_1, 0)$, $t_0 < t_1$. Therefore one can use a sprinkling map from $(x_1, x_2) \in [0, 1]^2$ to $(t, r) \in [t_0, t_1] \times [-(t_1 - t_0)/2, +(t_1 - t_0)/2]$ and reject points that lie outside the causal interval.

According to the by now well known procedure we start out by finding a map $f_1 : x_1 \mapsto t$ such that

$$V([t_0, t] \times [-(t_1 - t_0)/2, +(t_1 - t_0)/2]) = x_1 \cdot V([t_0, t_1] \times [-(t_1 - t_0)/2, +(t_1 - t_0)/2])$$

with

$$\begin{aligned} V([t_0, t] \times [-(t_1 - t_0)/2, +(t_1 - t_0)/2]) &= \int_{t_0}^{t} dt' \int_{-(t_1-t_0)/2}^{+(t_1-t_0)/2} dr \left(\frac{\alpha}{t'}\right)^2 \\ &= \int_{t_0}^{t} dt' \frac{\alpha^2 (t_1 - t_0)}{t'^2} \\ &= \alpha^2 (t_1 - t_0) \left(\frac{1}{t_0} - \frac{1}{t}\right). \end{aligned}$$

So one finds

$$t = \left(\frac{1}{t_0} - x_1 \left(\frac{1}{t_0} - \frac{1}{t_1}\right)\right)^{-1}. \tag{2.19}$$

As $\partial_r g_{\mu\nu} = 0$ one only needs to linearly map from $x_2 \in [0, 1]$ to $r \in [-(t_1 - t_0)/2, +(t_1 - t_0)/2]$. So one gets for the complete sprinkling map:

$$f : \begin{pmatrix} x_1 \\ x_2 \end{pmatrix} \to \begin{pmatrix} t = \left(\frac{1}{t_0} - x_1 \left(\frac{1}{t_0} - \frac{1}{t_1}\right)\right)^{-1} \\ r = (t_1 - t_0) \cdot (x_2 - 1/2) \end{pmatrix} \tag{2.20}$$

To sprinkle a single point one picks from $[0, 1]^2$ and uses f until one finds

$$(t, r) \in \{[t_0, t_1] \times \mathbb{R} \mid r \leq \min\{t_1 - t, t - t_0\}\}.$$

Like this we have avoided more complex integration over the causal interval. For later applications however the volume of the causal interval is still needed. Let the causal interval be in between

$x = (t_0, 0)$, $y = (t_1, r)$ with $t_1 - t_0 \geq |r|$ (there is translation symmetry along the spatial axis so this choice of coordinates is always possible). The causal interval will then be divided into three parts (see Fig. 2.1). Their respective volumes are

$$\begin{aligned}
V_1 &= \int_{t_0}^{t_0+T} dt \int_{-(t-t_0)}^{(t-t_0)} \left(\frac{\alpha}{t}\right)^2 \\
&= 2\alpha^2 \left(\log\left(\frac{t_0+T}{t_0}\right) - \frac{T}{t_0+T} \right) \\
V_2 &= \int_{t_0+T}^{t_1-T} dt\ (2T)\ \left(\frac{\alpha}{t}\right)^2 \\
&= 2\alpha^2 \left(\frac{T}{t_0+T} - \frac{T}{t_1-T} \right) \\
V_3 &= \int_{t_1-T}^{t_1} dt \int_{-(t_1-t)}^{(t_1-t)} \left(\frac{\alpha}{t}\right)^2 \\
&= 2\alpha^2 \left(\log\left(\frac{t_1-T}{t_1}\right) + \frac{T}{t_1-T} \right).
\end{aligned}$$

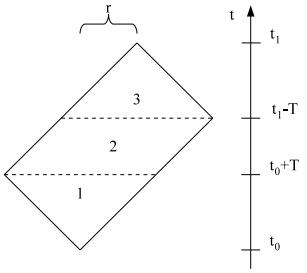

Figure 2.1: Three parts of a causal interval on de Sitter 2d: $T = (t_1 - t_0 - r)/2$

This yields an overall volume of

$$V(x, y) = 2\alpha^2 \ln\left(\frac{(t_1+t_0)^2 - r^2}{4\, t_0\, t_1}\right). \tag{2.21}$$

As can be verified easily the curvature scalar is

$$R = 2/\alpha^2. \tag{2.22}$$

2.4.5 Cylinder 2d

The cylinder spacetime is probably the easiest spacetime that exhibits non-trivial topology and is therefore a suitable object to study the corresponding effects on causal sets. Sprinkling into a cylinder spacetime is effectively the same as sprinkling into a rectangle on $\mathbb{M}^2$ with the exception that for the computation of the causal relations one must take into account the altered topology.

So for a cylinder with height T and circumference L and Cartesian coordinates (t, x) with all

$(t, x + n \cdot L)$ identified $\forall\ n \in \mathbb{Z}$ the easiest sprinkling map is

$$\begin{aligned} t &= T \cdot x_1 \\ x &= L \cdot x_2. \end{aligned} \tag{2.23}$$

As the shape of a causal interval on a cylinder strongly depends on the relative position of the two limiting points it is more convenient to always begin with a straightforward sprinkling into a rectangle containing the whole area and to reject unsuitable points afterwards.

Chapter 3

Propagators

3.1 Quantum Field Theory On Causal Sets

Eventually one would like to find a causal set based theory of everything that describes the behaviour of spacetime, matter and their mutual interaction. This means that in a "final" theory the matter living on a causal set must interact with the underlying set in a way that corresponds to what at the level of today's understanding is best described by Einstein's equations. Such a theory has not been found yet.

However it is considered an interesting exercise to construct a quantum field theory on a rigid causal set analogous to the way that quantum field theory is investigated on fixed background spacetimes to investigate effects like Hawking radiation of black holes. A natural starting point for this endeavour is real scalar field theory described by the Klein-Gordon equation. Steven Johnston has set out to find a procedure to determine the equivalent of the two point function of free real scalar field theory $\langle 0|T\{\phi(x)\phi(y)\}|0\rangle$ on a causal set. The method consists of two major steps: First one needs to find the equivalents for the advanced and retarded Green's functions of the Klein-Gordon equation and then one uses these functions to construct the Feynman propagator.[1] The second step is hoped to be independent of the structure of the causal set whereas the first step is at the moment only solved for flat Minkowski spacetime in two to four dimensions. A detailed description of how to get the Feynman propagator can be found in [8]. In [9] it is pointed out how the retarded Green's functions for two and four dimensional Minkowski spacetime are found by using a sum over paths approach which is a somewhat intuitive equivalent of the path integral formalism.

Unfortunately this procedure does not seem to work on general causal sets. There are strong hints that the presence of non-trivial topology and spacetime curvature require a separate treatment. The following sections do not solve these problems completely but shed some light on the situation and might help to reach a more complete solution.

[1] As pointed out in [8] the matrices for the advanced and retarded propagator are related by matrix transposition so one only needs to find one of the two.

Before we investigate the effects of non-trivial topology let us briefly state the main results for the Klein-Gordon propagator in $\mathbb{M}^2$ according to [9]: Consider the elements of the set labelled in some arbitrary order so that any element x_i can be referred to by some index i. The formula for the retarded propagator between two elements $x_i \prec x_j$ on a causal set corresponding to a causally convex patch of $\mathbb{M}^2$ is

$$\begin{aligned} K_{ij} &= \mathbb{I}_{ij} + a\,(A_C)_{ij} + a^2\,b\,\left(A_C^2\right)_{ij} + a^3\,b^2\,\left(A_C^3\right)_{ij} + \ldots \\ &= \mathbb{I}_{ij} + \sum_{n=1}^{\infty} a^n\,b^{n-1}\,(A_C^n)_{ij} \\ &= \left(\mathbb{I} + a\,A_C \cdot (1 - a\,b\,A_C)^{-1}\right)_{ij} \end{aligned} \tag{3.1}$$

with

$$(A_C)_{ij} = \begin{cases} 1 & \text{if } x_i \prec x_j \\ 0 & \text{else} \end{cases} . \tag{3.2}$$

In the context of causal sets A_C is sometimes referred to as the "causal matrix". $\mathbb{I}$ is the identity matrix with appropriate dimensions and $a = 1/2,\ b = -m^2/\rho$ with the mass m of the propagating particle and the sprinkling density ρ (cf. Sec. 2.2). The matrix element $\left(A_C^k\right)_{ij}$ gives the number of different ways to travel causally from x_i to x_j via k intermediate jumps. Therefore the sum in Eq. (3.1) can be understood as successively adding up the contributions from chains of increasing length (cf. Sec. 1.2). The causal set is locally finite which means that A_C is nilpotent and thus the sum eventually terminates. K is the causet equivalent of the retarded Klein-Gordon propagator in the sense that the expectation value of K_{ij} averaged over all sprinklings equals the value of the retarded continuum propagator evaluated at the positions of x_i and x_j for any non-zero density ρ.

3.2 The Cylinder Propagator

Let us now look at the retarded Klein-Gordon propagator on a cylinder spacetime with coordinates (t, r) with $(t, r + n \cdot L)\ \forall\ n \in \mathbb{Z}$ identified. The metric is $\eta_{\mu\nu}$ meaning that the cylinder is locally indistinguishable from $\mathbb{M}^2$.

Fig. 3.1a shows the propagator on the continuous manifold whereas Fig. 3.1b shows the discrete version according to Eq. (3.1) for comparison. The discrete version correctly approximates the continuum solution in the zones 0 and 1 (cf. Fig. 3.1d) but fails to do so in zones from 2 onwards. Zone 0 is spacelike to the perturbation origin at $(0, 0)$ and in both methods the propagator in these regions is explicitly set to 0 so the agreement is obvious. Zone 1 on its own is too small to be distinguishable from a patch of $\mathbb{M}^2$ yet: the topology is the same. So we expect anything that works on $\mathbb{M}^2$ to also work here. The situation changes fundamentally beyond that: Suddenly additional trajectories around the cylinder are causally accessible. This is precisely when the agreement between Figs. 3.1a and 3.1b breaks down.

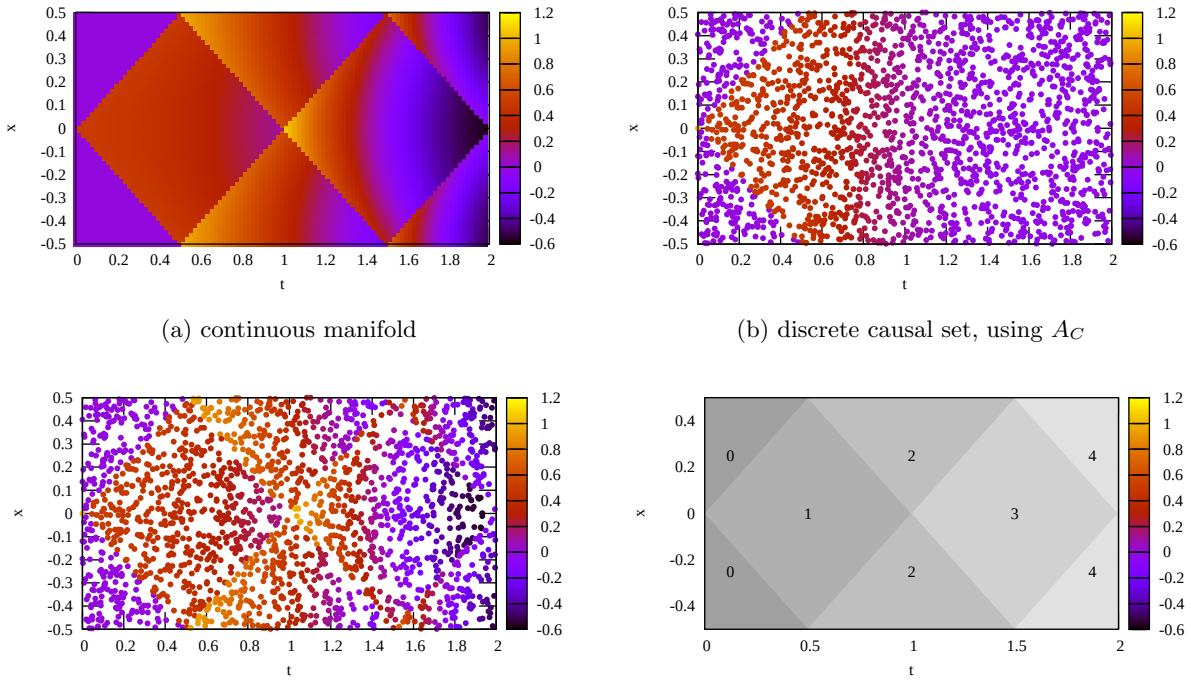

(a) continuous manifold

(b) discrete causal set, using A_C

(c) discrete causal set, using A_H

(d) different zones on cylinder

Figure 3.1: The retarded Klein-Gordon propagator on a cylinder with circumference $L = 1$, height $T = 2$, mass $m = 2$, perturbation origin at $(t = 0, r = 0)$ computed by different methods. For the discrete cases a single sprinkling with $N = 1000$ elements was used.

This is no big surprise: In the continuum case the propagator on $\mathbb{M}^2$ and the cylinder agree in zone 1 but beyond the extra contributions from the additional trajectories must be taken into account. This can readily be done by unrolling the cylinder and working in its covering space: Instead of the effect of a single perturbation at $(0, 0)$ on the cylinder one investigates the evolution of a whole series of perturbations at $(0, n \cdot L)\ \forall\ n \in \mathbb{Z}$ in regular $\mathbb{M}^2$. Due to the linearity of the Klein-Gordon equation and the principle of superposition these two cases can not be distinguished. Thus the cylinder propagator G_C from $y = (t_y, r_y)$ to $x = (t_x, r_x)$ is given by

$$G_C(y, x) = \sum_{n=-\infty}^{\infty} G_{\mathbb{M}^2}(y + (0, n \cdot L), x) \tag{3.3}$$

where $G_{\mathbb{M}^2}$ is the normal $\mathbb{M}^2$ propagator. In fact the labelling of the cylinder zones in Fig. 3.1d is the number of non-vanishing contributions in this sum.

Let us attempt the same approach for the causal set: Consider a sprinkling $\mathcal{C}$ into a cylinder spacetime with height T and circumference L. Now take a patch $(t, r) \in [0 : T] \times [-\infty, \infty]$ of $\mathbb{M}^2$ and create a causal set $\tilde{\mathcal{C}}$ by picking all the points $x_{i,n} = (t_i, r_i + n \cdot L)\ \forall\ n \in \mathbb{Z}, x_i = (t_i, r_i) \in \mathcal{C}$ from the patch with their induced order relations thereon.

To be precise $\tilde{\mathcal{C}}$ cannot be considered a real sprinkling as the placement of the points $x_{i,n}$ for different n is not independent and thus unwanted correlations in the probability distributions of

elements per volume occur. It is therefore not per se clear whether the instructions of Eq. (3.1) really give the appropriate propagator. One can treat the unrolled cylinder sprinkling in the same way as a proper $\mathbb{M}^2$ sprinkling as long as one does not evaluate probabilities that involve multiple instances of what was originally the same on the cylinder: Within a region of the covering space that does not include multiple instances of what was originally the same region on the cylinder everything looks like in a regular sprinkling. The probability distributions for two disjoint subsets of the covering space are just as uncorrelated as on a $\mathbb{M}^2$ sprinkling as long as they remain disjoint when one reintroduces the identification of points $(t, r + n \cdot L)\ \forall\ n \in \mathbb{Z}$.

Let $K_{ij}(\mathcal{C})$ denote the causet propagator matrix element (i, j) obtained from the causal set $\mathcal{C}$ by Eq. (3.1). To check whether $K_{(i,n)(j,m)}(\tilde{\mathcal{C}})$ gives the correct $\mathbb{M}^2$ equivalent propagator despite the correlations in $\tilde{\mathcal{C}}$ one must investigate the number of expected chains between the elements $x_{(i,n)}$ and $x_{(j,m)}$. On $\mathbb{M}^2$ the infinitesimal probability to find a chain between two given endpoints $y \prec x$ consisting of $n-1$ intermediate elements z_i in infinitesimal volumes d^2z_i is

$$\rho^{n-1} \prod_{i=1}^{n-1} d^2 z_i. \tag{3.4}$$

As the volume elements d^2z_i are infinitesimally small each of them can certainly be treated like regular sprinkling region and as the points z_i must be arranged in a causal order one can also be sure that multiple d^2z_i do not lie at different instances of what was originally the same location on the cylinder. Thus this density formula also holds for the pseudo sprinkling.

To get the overall number of expected chains with n intermediate jumps one must integrate over all possibilities. Let $I(y, x)$ denote the causal interval of two points $y \prec x$ on the sprinkling manifold. We have:

$$\left\langle \begin{matrix} \text{number of } n\text{-chains} \\ \text{between } y \text{ and } x \end{matrix} \right\rangle = \int_{I(y,x)} d^2 z_1 \int_{I(z_1,x)} d^2 z_2 \ldots \int_{I(z_{n-2},x)} d^2 z_{n-1}\ \rho^{n-1} \tag{3.5}$$

As the integration regions may be large enough to wrap around the cylinder the probability densities evaluated for different chains may be highly correlated. However for taking the mean of a sum of multiple random variables their mutual correlations are not relevant. Thus the number of expected chains of any length from y to x is the same for a $\mathbb{M}^2$ sprinkling and the pseudo sprinkling and therefore the propagators also give the same mean.

So in analogy to Eq. (3.3) we define the causet cylinder propagator between x_i and $x_j \in \mathcal{C}$ by summing up the causet propagators between $x_{i,n}$ and $x_{j,0}\ \forall\ n \in \mathbb{Z}$ on $\tilde{\mathcal{C}}$:

$$K(\mathcal{C})_{ij} := \sum_{n=-\infty}^{\infty} K(\tilde{\mathcal{C}})_{(i,n)(j,0)} \tag{3.6}$$

Let us look closer into the right-hand side of this equation:

$$\begin{aligned} K(\mathcal{C})_{ij} &= \sum_{n=-\infty}^{\infty} K(\tilde{\mathcal{C}})_{(i,n)(j,0)} \\ &= \sum_{n=-\infty}^{\infty} \left(\mathbb{I}_{(i,n)(j,0)} + \sum_{k=1}^{\infty} a^k \, b^{k-1} \, \left(A_C(\tilde{\mathcal{C}})^k \right)_{(i,n)(j,0)} \right) \\ &= \mathbb{I}_{ij} + \sum_{k=1}^{\infty} a^k \, b^{k-1} \sum_{n=-\infty}^{\infty} \left(A_C(\tilde{\mathcal{C}})^k \right)_{(i,n)(j,0)} \end{aligned} \tag{3.7}$$

where we have used the fact $\sum_n \mathbb{I}_{(i,n)(j,0)} = \mathbb{I}_{ij}$. Consider now the matrix

$$(A_H(\mathcal{C}))_{ij} := \sum_{n=-\infty}^{\infty} \left(A_C(\tilde{\mathcal{C}}) \right)_{(i,n)(j,0)} . \tag{3.8}$$

By taking its square we find

$$\begin{aligned} \left(A_H(\mathcal{C})^2 \right)_{ij} &= \sum_{m,n=-\infty}^{\infty} \sum_k \left(A_C(\tilde{\mathcal{C}}) \right)_{(i,n)(k,0)} \left(A_C(\tilde{\mathcal{C}}) \right)_{(k,m)(j,0)} \\ &= \sum_{m,n=-\infty}^{\infty} \sum_k \left(A_C(\tilde{\mathcal{C}}) \right)_{(i,n+m)(k,m)} \left(A_C(\tilde{\mathcal{C}}) \right)_{(k,m)(j,0)} \\ &= \sum_{m,n=-\infty}^{\infty} \sum_k \left(A_C(\tilde{\mathcal{C}}) \right)_{(i,n)(k,m)} \left(A_C(\tilde{\mathcal{C}}) \right)_{(k,m)(j,0)} \\ &= \sum_{n=-\infty}^{\infty} \left(A_C(\tilde{\mathcal{C}})^2 \right)_{(i,n)(j,0)} \end{aligned} \tag{3.9}$$

where the sum over k runs over all labelling indices of $\mathcal{C}$ and the discrete translation symmetry of $\tilde{\mathcal{C}}$ induced by unrolling the cylinder was used when setting $\left(A_C(\tilde{\mathcal{C}}) \right)_{(i,n)(k,0)} = \left(A_C(\tilde{\mathcal{C}}) \right)_{(i,n+m)(k,m)}$. This calculation runs through for all higher powers of A_H and thus we can rewrite Eq. (3.7) as

$$K(\mathcal{C})_{ij} = \mathbb{I}_{ij} + \sum_{k=1}^{\infty} a^k \, b^{k-1} \left(A_H(\mathcal{C})^k \right)_{ij} \tag{3.10}$$

which is of the very same form as Eq. (3.1) except that A_C is replaced by the new A_H. Comparison between Fig. 3.1a and 3.1c indicates that the new propagator is indeed working on the whole cylinder.

$(A_H)_{ij}$ counts the number of copies of the initial perturbation source located at x_i that are "visible" at x_j. This is equal to the number of equivalence classes of causal trajectories from x_i to x_j where two trajectories are considered equivalent when they are homotopic. Therefore A_H will be referred to as the *homotopy matrix*.

3.3 Non-trivial Topology In Four Dimensions

To see how general the concept of the homotopy matrix is let us now consider a simple setup in four dimensions. One starts out with regular $\mathbb{M}^4$. The retarded causet propagator thereon is found in a way quite similar to Eq. (3.1) only this time one must not use the causal matrix but what is known

as the link matrix. For $\mathbb{M}^4$ one has [9]:

$$\begin{aligned} K_{ij} &= \left(\mathbb{I} + a\, A_R \cdot (1 - a\, b\, A_R)^{-1}\right)_{ij} \qquad (3.11) \\ &\text{with} \\ (A_R)_{ij} &= \begin{cases} 1 & \text{if } x_i \prec\!\!\!\cdot\, x_j \\ 0 & \text{else} \end{cases} \\ a &= \frac{\sqrt{\rho}}{2\pi\sqrt{6}} \\ b &= -\frac{m^2}{\rho} \end{aligned}$$

So one does not sum over all ways to travel from x_i to x_j but only over those with jumps between nearest neighbours, i.e. paths (cf. Sec. 1.2). This propagator will correctly approximate the continuum propagator only in the limit of high density ρ.

Now consider the compactification of one spatial dimension: Let $\mathcal{M}_1$ be the manifold obtained by taking $(t, r_1, r_2, r_3) \in \mathbb{M}^4$ with (t, r_1, r_2, r_3) and $(t, r_1 + n \cdot L, r_2, r_3)$ identified $\forall\ n \in \mathbb{Z}$ and the flat metric $\eta_{\mu\nu}$ thereon. On the continuum an elegant way to find the propagator is again to go into the covering space and sum over an appropriate set of $\mathbb{M}^4$ propagators. The retarded propagator $G_{\mathcal{M}_1}(y, x)$ for the amplitude from y to x is

$$G_{\mathcal{M}_1}(y, x) = \sum_{n=-\infty}^{\infty} G_{\mathbb{M}^4}(y + (0, n \cdot L, 0, 0), x)$$

where $G_{\mathbb{M}^4}$ is the regular retarded $\mathbb{M}^4$ propagator.

Again we like to apply the same technique for the discrete case thus we again need an "unrolling" $\tilde{\mathcal{C}}$ of a sprinkling $\mathcal{C}$ into $\mathcal{M}_1$ which can be created by

$$\tilde{\mathcal{C}} = \{x_{i,n} = (t_i, r_{i,1} + n \cdot L, r_{i,2}, r_{i,3}) \mid \forall\ x_i = (t_i, r_{i,1}, r_{i,2}, r_{i,3}) \in \mathcal{C}, \forall\ n \in \mathbb{Z}\}$$

with causal relations implied by $\mathbb{M}^4$.

At this point it shall be emphasized once more that this is not a valid causal set operation. We are cheating as we are remembering the original positions of the set elements on the sprinkling manifold. For the sake of gaining a better understanding of things one may ignore the rules. But an operation like this is not allowed to be part of a final causal set theory.

The next step is to check whether the pseudo sprinkling $\tilde{\mathcal{C}}$ gives the correct retarded $\mathbb{M}^4$ causet propagator via Eq. (3.11). Like on the cylinder the pseudo sprinkling obeys the same statistics as a regular sprinkling as long as one does not "abuse" the fact that it was created by unrolling. In four dimensions one does not sum over all chains but only over paths. So relative to the 2d probability density for all chains Eq. (3.4) an extra factor for the probability that the causal volume between two successive elements is empty must be added. The infinitesimal probability to find a path between

given y and x with $n-1$ intermediate elements is

$$\rho^{n-1}\prod_{i=1}^{n-1} d^4 z_i \cdot \mathrm{P}(n(y,z_1)=0)\cdot \prod_{i=1}^{n-2}\mathrm{P}(n(z_i,z_{i+1})=0)\cdot \mathrm{P}(n(z_{n-1},x)=0). \tag{3.12}$$

On $\mathbb{M}^4$ one has $\mathrm{P}(n(z_i,z_{i+1})=0)=\exp(-\rho\, V(z_i,z_{i+1}))$. This is not always true for the pseudo sprinkling: When y and x are far enough apart paths must be considered where two successive elements z_i, z_{i+1} are so far apart that their intermediate causal volume actually reaches the regime where the correlations induced by the unrolling process kick in. For these paths the probability formula must be altered. Only a corrected volume which does not measure any same cylinder regions twice must be considered. However for this corrections to become necessary the intermediate volume (on $\mathbb{M}^4$ and the corrected version) must be at least of the order L^4 and thus the path contribution will be suppressed with an exponential $\exp(-\rho\,\mathcal{O}(L^4))$. As the propagator only works in the high density limit anyway paths where these corrections become necessary are negligible compared to paths where the causal volume between all successive elements is small. The integration to sum the total probability over all paths is not affected by correlations just like in the 2d case. So again the pseudo sprinkling will give the right propagator although this time it is only a (very good) approximation.

So exactly as in Eq. (3.6) the causet propagator for $\mathcal{M}_1$ sprinklings will be defined as

$$K(\mathcal{C})_{ij} := \sum_{n=-\infty}^{\infty} K(\tilde{\mathcal{C}})_{(i,n)(j,0)}. \tag{3.13}$$

The same procedure as in Eqns. (3.7) to (3.10) is applicable only here one needs what will be dubbed the *homotopy link matrix* $A_W(\mathcal{C})$ instead of $A_H(\mathcal{C})$ which is defined by:[2]

$$(A_W(\mathcal{C}))_{ij} := \sum_{n=-\infty}^{\infty} \left(A_R(\tilde{\mathcal{C}})\right)_{(i,n)(j,0)} \tag{3.14}$$

So one finds

$$K(\mathcal{C})_{ij} = \mathbb{I}_{ij} + \sum_{k=1}^{\infty} a^k\, b^{k-1} \left(A_W(\mathcal{C})^k\right)_{ij} \tag{3.15}$$

for sprinklings into $\mathcal{M}_1$.

3.4 Propagators And The Fundamental Homotopy Group

Consider the following premises: Let $\mathcal{M}$ be an n-dimensional Lorentzian manifold (with good enough causality conditions to do QFT thereon) which has a universal covering space $\mathcal{N}$ with a covering map $f:\mathcal{N}\to\mathcal{M}$. Assume both $\mathcal{M}$ and $\mathcal{N}$ are path connected. In the continuum case the retarded propagation amplitude $G_{\mathcal{M}}(y,x)$ between two points y and x on $\mathcal{M}$ can be computed by summing up the amplitudes $G_{\mathcal{N}}(y_i,x_0)$ of the retarded propagator on $\mathcal{N}$ for all $y_i\in\mathcal{N}$ such that $f(y_i)=y$ and a fixed $x_0\in\mathcal{N}$ such that $f(x_0)=x$. The causet propagator for a sprinkling on $\mathcal{N}$ can be computed by using a sum over chains and/or paths.

[2]The letter W was chosen as subscript because it has the same relative position to R in the alphabet as H has to C

Under these conditions for a sprinkling $\mathcal{C}$ into $\mathcal{M}$ there is a pseudo sprinkling $\tilde{\mathcal{C}} = \{z_{i,n} \mid f(z_{i,n}) = z_i \ \forall \ z_i \in \mathcal{C}\}$ on $\mathcal{N}$. The elements $z_{i,n} \in \tilde{\mathcal{C}}$ that satisfy $f(z_{i,n}) = z_i$ will be called instances of $z_i \in \mathcal{C}$. In analogy (metric determinants must be inserted) to Eqns. (3.4) and (3.12) the set $\tilde{\mathcal{C}}$ will yield the same number of expected chains and in the limit of $\rho\, l_t^2 \gg 1$ the same number of expected paths as a real sprinkling onto $\mathcal{N}$. Here l_t is the length scale from which on the potentially non-trivial topology of $\mathcal{M}$ is relevant. Thus a propagator built from sums over paths and/or chains will give the same expectation value. The retarded causet propagator between two elements z_i and $z_j \in \mathcal{C}$ is defined by summing up the causet propagators from all instances of z_i to a fixed instance of z_j.

There is a bijection between the instances $z_{i,n}$ of z_i and the fundamental group of $\mathcal{M}$. Pick out one instance $z_{i,0}$ and choose a set of paths from $z_{i,0}$ to all other $z_{i,n}$. As $\mathcal{N}$ is simply connected all paths between the same endpoints $z_{i,0}$ and $z_{i,n}$ will be homotopic. Now take a $z_{i,n}$ and a corresponding path and consider the projection of that path onto $\mathcal{M}$ via f. As $f(z_{i,0}) = f(z_{i,n}) = z_i$ this path is now a loop. This loop can be identified with an element of the fundamental homotopy group of $\mathcal{M}$. As for any two paths linking $z_{i,0}$ and $z_{i,n}$ there is a (endpoint fixing) homotopy Γ continuously deforming one into the other also the two corresponding projected loops on $\mathcal{M}$ via f will be homotopic with a homotopy $f \circ \Gamma$. So there is a unique element of the fundamental group of $\mathcal{M}$ that can be associated with $z_{i,n}$.

Consider now two different instances $z_{i,n}$ and $z_{i,m}$ with respective paths from $z_{i,0}$ on $\mathcal{N}$. If the two projected loops on $\mathcal{M}$ were homotopic the lifting property (see for example [10]) would induce a homotopy of the two original paths on $\mathcal{N}$ which cannot exist as both paths have different ending points. Thus different instances must be assigned different elements in the homotopy group.

Finally pick any element of the homotopy group and a representative loop at z_i on $\mathcal{M}$. Lift this loop at the instance $z_{i,0}$ to $\mathcal{N}$ and it will become a path to some $z_{i,n}$ i.e. for any homotopy class there is a corresponding instance.

In summary, there is a map from the instances $z_{i,n}$ to the elements of the homotopy group of $\mathcal{M}$. This map is both injective and surjective and hence a bijection.

Both the cylinder in Sec. 3.2 and the manifold $\mathcal{M}_1$ in Sec. 3.3 are examples of what is described here. Indeed the sums in the definitions of the homotopy matrices A_H and A_W in Eqns. (3.8) and (3.14) can be interpreted as sums over the homotopy groups which are in both cases isomorphic to the integers under addition $\mathbb{Z}$. $\mathbb{M}^4$ with two and three compactified spatial dimensions are two additional examples with homotopy groups that are isomorphic to $\mathbb{Z}^2$ and $\mathbb{Z}^3$ respectively.

3.5 Propagators And Curvature: 2d

All two dimensional spacetimes are conformally flat so there is always a coordinate system in which the metric is of the form $g_{\mu\nu} = \omega\, \eta_{\mu\nu}$ where ω is a positive function of the coordinates.

Consider now the d-dimensional Klein-Gordon equation $(\Box + m^2)\phi = 0$ and the d'Alembertian

$$\begin{aligned}\Box\phi &= g^{\mu\nu}\nabla_\mu\nabla_\nu\phi \\ &= g^{\mu\nu}\left(\partial_\mu\partial_\nu - \Gamma^\alpha_{\mu\nu}\partial_\alpha\right)\phi\end{aligned}$$

where $\Gamma^\alpha_{\mu\nu}$ is the Christoffel symbol. For a conformally flat metric $g_{\mu\nu} = \omega\,\eta_{\mu\nu}$ this simplifies to

$$\begin{aligned}\Box\phi &= g^{\mu\nu}\left(\partial_\mu\partial_\nu - \Gamma^\alpha_{\mu\nu}\partial_\alpha\right)\phi \\ &= \left(\omega^{-1}\eta^{\mu\nu}\partial_\mu\partial_\nu - \frac{1}{2\omega^2}(2-d)\eta^{\mu\nu}(\partial_\mu\omega)\partial_\nu\right)\phi\end{aligned}$$

For $d = 2$ one has $\Box\phi = g^{\mu\nu}\partial_\mu\partial_\nu\phi$. In the presence of curvature the Dirac delta distribution that describes a perturbation on the right-hand side of the Klein-Gordon equation must be added an extra factor of $\sqrt{-g}^{-1}$ so that $\int d^dx\sqrt{-g}\delta^{(d)}_g(x - x_0)$ is invariant of choice of coordinates with $\delta^{(d)}_g(x) = \sqrt{-g}^{-1}\,\delta^{(d)}(x - x_0)$ and $\delta^{(d)}$ being the d-dimensional Dirac delta distribution. In conformally flat coordinates $\sqrt{-g} = \omega^{d/2}$. So for two dimensions the equation that needs to be solved for finding the massless propagators in conformally flat coordinates is

$$\omega^{-1}\eta^{\mu\nu}\partial_\mu\partial_\nu G(x - y) = \omega^{-1}\delta^{(2)}(x - y).$$

The factor ω^{-1} cancels and thus the equation takes the same form as in flat $\mathbb{M}^2$. Thus in conformally flat coordinates which we choose to be called (t, r) just as in $\mathbb{M}^2$ the retarded massless propagator is given by the same mathematical function of these coordinates t and r. Thus we know that the massless causet propagator still works.

Let us now deal with the massive case: Given the massless retarded continuum propagator $G(y, x) = G(x - y)$ from y to x the massive propagator $G_m(y, x)$ can be constructed as a perturbation series given by

$$G_m(y, x) = G(y, x) - m^2(G.G)(y, x) + m^4(G.G.G)(y, x) - \ldots \tag{3.16}$$

with $(A.B)(y, x) = \int d^2z\sqrt{-g(z)}\,A(y, z)B(z, x)$. As the massive propagator is in general no longer translation invariant it is no longer a function of $x - y$ (except of course if ω is translation invariant).

Consider now the massless causet propagator $K_{ij} = a(A_C)_{ij}$ with $a = 1/2$ and the series

$$K_{m,ij} = a(A_C)_{ij} + a^2b\,((A_C)^2)_{ij} + a^3b^2\,((A_C)^3)_{ij} + \ldots \tag{3.17}$$

with $b = -m^2/\rho$ which gave us the massive propagator on $\mathbb{M}^2$ (cf. Eq. (3.1) where we drop the identity for now as it does not describe actual propagation). What is the expectation value of $\langle K_{m,xy}\rangle$ for two points labelled by x_i and x_j that we assume to be elements of the causal set? For that we need to know the expectation values $\langle(A^n_C)_{ij}\rangle$. This is the expected number of chains from x_i to x_j with n intermediate jumps which was computed for $\mathbb{M}^2$ in Eq. (3.5). For conformally flat spacetimes we need to insert a metric determinant at each intermediate element z_i.

$$\langle(A^n_C)_{ij}\rangle = \int_{I(x_i,x_j)} d^2z_1 \int_{I(z_1,x_j)} d^2z_2 \ldots \int_{I(z_{n-2},x_j)} d^2z_{n-1}\,\rho^{n-1}\prod_{k=1}^{n-1}\sqrt{-g(z_k)} \tag{3.18}$$

Let now all integrals go over the whole manifold and insert factors $\langle (A_C)_{\#(z_i)\#(z_{i+1})} \rangle$ at each jump.[3] This is the trivial probability for the existence of a chain with one jump between two elements z_i and z_{i+1} given these elements are in the sprinkling. It is 1 if $z_i \prec z_{i+1}$ and 0 otherwise. Hence Eq. (3.18) can be written as

$$\langle (A_C^n) \rangle (x_i, x_j) = \underbrace{(\langle A_C \rangle . \langle A_C \rangle \dots \langle A_C \rangle)}_{n \text{ convoluted factors}} (x_i, x_j) \cdot \rho^{n-1} \tag{3.19}$$

where x_i and x_j have been denoted as regular continuous arguments here as we assume $x_i, x_j \in \mathcal{C}$ for any x_i, x_j that we want to look at and thus can treat them as continuous arguments.

Putting all this together one can write the expectation value for $\langle K_{m,ij} \rangle$ on conformally flat spacetimes as

$$\langle K_m \rangle (y, x) = G(y, x) - m^2 (G.G)(y, x) + m^4 (G.G.G)(y, x) - \dots \tag{3.20}$$

where we have used $a\langle A_C \rangle (x_i, x_j) = \langle K \rangle (x_i, x_j) = G(x_i, x_j)$ for the massless propagators and that the powers of ρ from the denominator of b cancel with those from the expected number of chains. This is the same as the massive continuum propagator.

Note that the validity of Eq. (3.19) does not rely on the fact that $\langle A_C \rangle$ is so very simple and basically only serves as effective limitation of the integration regions. It is sufficient that the random variables in the single convolution factors are uncorrelated which they automatically are because they describe propagation in non-intersecting regions. So the causet equivalent Eq. (3.17) of the perturbation series Eq. (3.16) can also be used to find solutions to other additional terms in the Klein-Gordon equation as long as their causet equivalent is known.

So we know that the procedure to get both the massless and the massive causet propagator according to Eq. 3.1 still works in the presence of curvature for trivial topology in two dimensions and additionally for all non-trivial topologies where Sec. (3.4) applies.

A curious example of this is two dimensional de Sitter space which has the topology of a cylinder. So one would be able to apply the homotopy matrix method. However the non-trivial paths are concealed by causality so there are no zones $H_x(n > 1)$ for any x, the non-trivial topology is not visible and one finds $A_H = A_C$. This is why the discussion of de Sitter space can be so readily performed in conformally flat coordinates that do not contain the information about the cylinder topology [7].

3.6 Propagators And Curvature: 4d

In four dimensions the situation is considerably more difficult. Not all spacetimes are conformally flat. Moreover the form of the d'Alembertian in the conformally flat case is not as simple as in 2d. Using a conformally coupled d'Alembertian some special cases can still be solved. This section however focuses

[3] $\#(z_i)$ is a function to obtain the index of the element z_i in the x_i labelling.

on the general case and examines if the retarded causet propagator given by Eq. 3.11 for $m = 0$ does still approximate the continuum propagator correctly in general curved four dimensional spacetimes.

For general spacetimes obtaining the continuous retarded propagator analytically is an intractable task. In [11] an explicit method to construct the retarded propagator for a large class of spacetimes is given but it is still not straightforwardly applicable in practice. However this method teaches us some things about the form of the solution. It is shown that the retarded massless propagator can be decomposed into a singular part that lives on the future lightcone of the perturbation and a tail that lives within. For $m = 0$ we can see right away that the causet propagator does not posses a tail as it is only non-zero on the elements that are linked to the perturbation and these elements will cling to the lightcone with increasing density. However the singular part is also not approximated correctly. According to [11] the singular part of the retarded propagator from x to y can be written as $G_{\text{singular}}(x, y) = U(x, y)\delta_+(\sigma(x, y))$ where $\sigma(x, y)$ is the Synge world function and δ_+ is the Dirac-delta limited to the future of y by a step function which is 1 if x is to the future of a spacelike hypersurface that contains y. This sounds rather complicated but it is just picking out the future light cone of y. It is shown that the function $U(x, y) = \Delta^{1/2}(x, y)$ where $\Delta(x, y)$ is the van Vleck determinant.

In $\mathbb{M}^4$ the coefficient U is given by $U = 1/(4\pi)$. In [9] it is shown that this is correctly approximated by the causet propagator in the mean. It is tricky to investigate the value of the coefficient of a delta-singularity. For $\mathbb{M}^4$ this problem was overcome by switching to the Fourier space where the singularity is avoided. However Fourier transformation is not as powerful in general spacetimes as there is not always a known set of complete functions let alone that it is so simple as the plane waves in flat space. An alternative approach that works in the space domain shall be introduced here.

Let us start by noting that a continuum propagator is only well defined as a distribution and therefore one must investigate the effect of two propagators as distributions in an integral and not their "function values". On a causal set integration over a volume corresponds to summing up values at different elements multiplied with the Planckian volume. When comparing the effect of a causet propagator to a continuum propagator as a distribution on a space of functions one can either port the continuous test functions to the causal set by taking $\phi_x = \phi(x)$ or one can port the causet propagator of $\mathcal{C}$ onto the continuum via

$$G_{\text{causet}}(y, x) = \sum_{z \in \mathcal{C}} K_{yz}(\mathcal{C})\, V_p \sqrt{-g}^{-1}\, \delta^{(4)}(x - z).$$

This must be interpreted as follows: y must be an element of $\mathcal{C}$ and $V_p = \rho^{-1}$ is the Planckian volume. K_{yz} gives the causet propagation amplitude from y to z and the symbol z in the δ-distribution refers to the coordinates of z on the continuous manifold. Evaluating a continuous volume integral with a test function and this propagator will yield the same result as porting the test function onto the set and perform the discrete integral equivalent there. For the massless case the expectation value of

G_{causet} for a sprinkling assuming that y is always contained in the set is:

$$\begin{aligned}\langle G_{\text{causet}}(y,x)\rangle &= \int_{J^+(y)} d^4z\,\sqrt{-g}\,\rho\;(a\,\exp(-\rho\,V(y,z)))\;V_p\,\sqrt{g}^{-1}\delta^{(4)}(x-z)\\ &= \begin{cases} a\,\exp(-\rho\,V(y,x)) & \text{for } x\in J^+(y)\\ 0 & \text{else}\end{cases}\end{aligned} \tag{3.21}$$

Here $J^+(y)$ denotes the causal future of y, $d^4z\,\sqrt{-g}\,\rho$ is the infinitesimal probability to find a set element at z, $(a\,\exp(-\rho\,V(y,z)))$ is the expectation value for the matrix element K_{yz} where the contribution of the identity matrix (see Eq. (3.11)) has been dropped as it does not describe actual propagation. As distributions are linear maps one can take this expectation value as the kernel in test function integrals to get the expectation value of the integral.

As the continuum propagators contain $\delta(\sigma)$-singularities let us investigate the effect of the ported causet propagator on integrals along the gradient of the Synge world function. We will start with $\mathbb{M}^4$. According to the conventions in [11] $\sigma(y,x) = -\tau(y,x)^2/2$ and for $\mathbb{M}^4$ we have $V(y,x) = \pi\tau(y,x)^4/24 = \pi\sigma(y,x)^2/6$ where $\tau(y,x)$ is the eigentime distance between y and x for $y \prec x$.

So let us pick a contour through a point x_0 on the future lightcone of y which moves along the gradient of the Synge world function. The contour will be given by a function $x(\lambda)$ with $x(0) = x_0$ and $\sigma(y, x(\lambda)) = \lambda$. We will integrate the product of the expectation value of the ported propagator Eq. (3.21) and a test function $h(x)$ in the limit of high sprinkling density ρ (as only then the propagator is expected to work) along a part of the contour that contains x_0. The integral is

$$I = \lim_{\rho\to\infty}\int_{\lambda_a}^{\lambda_b} d\lambda\, h(x(\lambda))\,\langle G_{\text{causet}}(y, x(\lambda))\rangle$$

with $\lambda < 0, \lambda > 0$. Assume $h(x(\lambda))$ can be expanded in orders of λ around $h(x(0))$ in a series $h(x(\lambda)) = \sum_{k=0}^{\infty} h_k\lambda^k$. Then we have

$$\begin{aligned} I &= \lim_{\rho\to\infty}\int_0^{\lambda_b} d\lambda\,(h_0 + \mathcal{O}(\lambda))\,a\,\exp(-\rho\pi\lambda^2/6)\\ &= \lim_{\rho\to\infty} h_0\,\frac{a}{2}\,\sqrt{\frac{6}{\rho}}\end{aligned} \tag{3.22}$$

For the continuum $\mathbb{M}^4$ propagator one would obtain $I = h_0/(4\pi)$. So for both versions to coincide one indeed needs to set $a = \frac{1}{2\pi}\sqrt{\frac{\rho}{6}}$ as derived via Fourier transform.

Now let us look at what happens in the presence of curvature. We assume that x_0 and an open set containing x_0 are in a *convex normal neighbourhood* of y which is the region where points are linked to y by unique geodesics [11]. This is required to make sure that σ is a suitable integration parameter around x_0. In [12] the corrections to the volume of a causal interval on a four dimensional manifold are given compared to the flat Minkowskian case. For us the relevant part is that the coefficient of the leading order of σ is not changed. Hence the integral Eq. (3.22) will not change in the limit $\rho \to \infty$. Therefore the singularity coefficient U given by the causet propagator will also be constant in the

presence of curvature (at least near the perturbation origin where the volume formulas given in [12] hold) which does not agree with the desired continuum result.

Thus unlike in two dimensions here additional rules to cope with curvature are required. In $\mathbb{M}^4$ the fact was used that the links of y cling to the future lightcone of y to model the singular part. In the presence of curvature the singular part is no longer constant but depends on an integral along a null geodesic in the lightcone. If one would like to model this integration one must first extend the notion of lightcones on causal sets as the set of links themselves has no internal structure so a geodesic cannot be modelled therein.

Chapter 4

Topology

4.1 Recovering Topology From The Causal Set

The quest for the cylinder propagator in Sec. 3.2 has shown that it is necessary to recover the topology of the original manifold from the causal set. As mentioned in Sec. 2.1 it has been proven [2, 3, 4] that the causal structure of the points of a future and past distinguishing Lorentzian manifold is enough to determine its topology. Therefore for high sprinkling densities one expects the topology to be somehow encoded in the causal set. Thus it should be possible to approximately recover the homotopy matrix A_H from the causal matrix A_C.

Of course this is not a new problem and there are already promising approaches to recovering the continuum topology from the causal set: For example in [1] a simplicial complex is constructed from a thickened maximal antichain and it is shown that the Betti numbers of this complex coincide with the ones from the original manifold in a certain range of thickening-depth.

For one thing the author of this thesis has a certain aversion to the introduction of new intermediate length scales like the thickening-depth. So the potential of methods that do not need a new length scale should be carefully examined. For another thing the method presented in [1] focuses on the detection of the topology of a given set without taking into account causal accessibility which must be considered for the problem in question.

This chapter will discuss approaches to an algorithm that can approximately recover the homotopy matrix A_H from the causal matrix A_C on sprinklings into some Lorentzian manifolds. For two given points $x \prec y$ one must find the number of equivalence classes of causal paths from x to y where two paths will be considered equivalent when they are homotopic.

4.2 Intersecting Lightcones

In this section an algorithm will be discussed that can approximately recover the homotopy matrix A_H from the causal matrix A_C on sprinklings into the cylinder manifold (see Sec. 2.4.5).

For a manifold $\mathcal{M}$ the symbols $J^{+,-}(x)$ will refer to the causal future or past of a given point x on $\mathcal{M}$ where we adopt the convention that $x \in J^{+,-}(x)$. $\tilde{J}^{+,-}(x)$ will refer to the lightcone only i.e. $\tilde{J}^{+,-}(x)$ is the subset of $J^{+,-}(x)$ that has zero eigentime distance from x. The eigentime distance of two points is integrated along a geodesic linking the points. In case there are multiple geodesics like on the cylinder the smallest possible eigentime will be chosen. $H_x(n)$ will refer to the set of points $y \subset J^+(x)$ such that between x and y there are n equivalence classes of causal trajectories.

Let us first discuss how the zones $H_x(n)$ can be identified on the continuous cylinder manifold. Note how the set $\tilde{J}^+(x)$ forms a grid wrapping around the cylinder that separates the different homotopy zones $H_x(n)$ (cf. Fig. 3.1d). This is understandable as each time one crosses a branch of the lightcone a new class of paths becomes accessible and one skips to the next zone $H_x(n+1)$. The point where zones $H_x(1)$ and $H_x(3)$ meet can be interpreted as simultaneous crossing of two branches.

The first point that can be reached from x via two separate paths is z_1 where the two light cone branches intersect for the first time after emerging from x. All other points of $H_x(2)$ lie to the future of that point. In fact any point to the future of z_1 is in some $H_x(n)$ for $n > 1$ and no point in the past of z is in some $H_x(n)$ for $n > 1$. So

$$H_x(1) = J^+(x) \setminus J^+(z_1). \tag{4.1}$$

After the two branches meet at z_1 they set out on another turn around the cylinder and will intersect again at z_2. Therefore one finds on a cylinder that $H_x(n+1) = H_{z_1}(n)$ and thus that

$$H_x(n \mid n > 1) = J^+(z_{n-1}) \setminus J^+(z_n). \tag{4.2}$$

When trying to port these rules to the causal set $\mathcal{C}$ obtained by sprinkling on the cylinder one faces two difficulties: On a causal set there is no exact correspondence to the lightcones thus the identification of the points z_i is complicated. To make things worse the probability that any of the intersection points z_i is chosen for the sprinkling is zero. So the rules given above cannot be applied as is.

Recall that $J^+(z)$ on $\mathcal{M}$ can be written as

$$J^+(z) = \bigcap_{y \in \Omega} J^+(y) \tag{4.3}$$

for an arbitrary set $\Omega \subset J^-(z)$ such that $z \in \Omega$. In particular $J^+(z_1)$ is the intersection of the futures of all $y \in \Omega_x(1) = \tilde{J}^+(x) \cap \tilde{J}^-(z_1)$ that is the piece of the future lightcone of x that connects x and z_1. For $\Omega_x(1)$ there is an approximate equivalent on a causal set: Consider the set of sprinkled elements that are future links of x i.e. $\{y \in \mathcal{C} \mid x \prec y \wedge n(x,y) = 0\}$. The corresponding probability density for such a point to be placed at $y \succ x$ during a sprinkling is given by $\rho \cdot \mathrm{P}(n(x,y) = 0) = \rho \exp(-\rho\, V(x,y))$. For high densities this distribution becomes concentrated in areas with small $V(x,y)$ which is a small

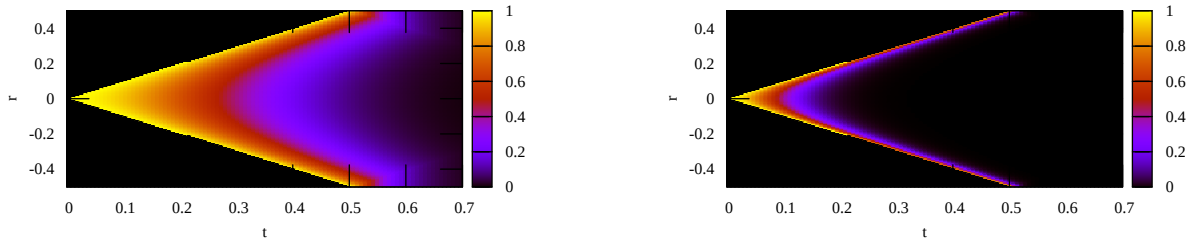

(a) $\rho = 20$ (b) $\rho = 200$

Figure 4.1: The function $\exp(-\rho V(x, y))$ for $x = (0, 0), y = (t, r)$ on the cylinder manifold for different ρ. This function determines the shape of the future link density of x. For large ρ it is only non-zero along the lightcone from x to $z = (0.5, 0.5) \equiv (0.5, -0.5)$

region that clings to the lightcone between x and z_1 (see Fig. 4.1). So a potential replacement of Eq. (4.1) is

$$\begin{aligned} H_x(1) &= J^+(x) \setminus \left(\bigcap_{y \in \Omega_x(1)} J^+(y) \right) \qquad (4.4) \\ &\text{with} \\ \Omega_x(1) &= \{y \in J^+(x) \mid n(x, y) = 0\} \\ J^+(x) &= \{y \in \mathcal{C} \mid x \prec y\}. \end{aligned}$$

Note that in a slight abuse of notation the symbols $H_x(1), \Omega_x(1)$ and $J^+(x)$ are now used for subsets of the sprinkling $\mathcal{C}$ into $\mathcal{M}$. Each of them is clearly an attempt to model what is described by the same symbol on $\mathcal{M}$ itself so the double use of the symbols should not be too confusing. Be however aware of the subtle difference of $J^+(x)$ on the causet and on the manifold: $x \notin J^+(x)$ on $\mathcal{C}$ but $x \in J^+(x)$ on $\mathcal{M}$.

On the continuum the next step was to swap x for z_1 and z_1 for z_2 to get $H_x(2)$ (cf. Eq. (4.2)). This cannot be done here. Think of the properties a point z_1 that was part of the sprinkling would need: it would have to be to the past of every point in $J^+(x) \setminus H_x(1)$ but none of the points of $H_x(1)$ would be in its future. Then we would use the future links of that point to construct what would be the future of z_2 just as with the set $\Omega_x(1)$ in Eq. (4.4). Given such a hypothetical point z_1 one would construct $\Omega_x(2) = \{y \in J^+(x) \mid n(z_1, y) = 0\}$ and

$$H_x(2) = H_{z_1}(1) = J^+(z_1) \setminus \left(\bigcap_{y \in \Omega_x(2)} J^+(y) \right)$$

as above. Luckily one does not need the point z_1 itself to be able to get $H_x(2)$: what would be $J^+(z_1)$

can be obtained by taking $J^+(x) \setminus H_x(1)$ and

$$\begin{aligned} \Omega_x(2) &= \{y \in H_x^+(2) \mid J^-(y) \cap H_x^+(2) = \emptyset\} \\ &\text{with} \\ H_x^+(n) &= J^+(x) \setminus \bigcup_{k=1}^{n-1} H_x(k). \end{aligned} \tag{4.5}$$

This means $\Omega_x(2)$ is the subset of elements in $H_x^+(2) = J^+(x) \setminus H_x(1)$ that are minimal in $H_x^+(2)$. Under this condition they would be future links of the hypothetical element z_1. Note that here also the convention $y \notin J^-(y)$ has been chosen for the causal set. Combining all this one finds that higher order zones are obtained by

$$\begin{aligned} H_x(n) &= H_x^+(n) \setminus \left(\bigcap_{y \in \Omega_x(n)} J^+(y) \right) \\ &\text{with} \\ \Omega_x(n) &= \left\{ y \in H_x^+(n) \mid J^-(y) \cap H_x^+(n) = \emptyset \right\}. \end{aligned} \tag{4.6}$$

$\Omega_x(n)$ is the set of minimal elements in $H_x^+(n)$. It can be verified that this is a consistent successive construction of the zones that at each step only requires information that already is available. Knowing all sets $H_x(n)$ for all $x \in \mathcal{C}$ it is easy to write down the homotopy matrix A_H.

Unfortunately when applying this algorithm to actual cylinder sprinklings it turns out not to work as well as was hoped (cf. Fig. 4.2a). Although the probability density for the points in $\Omega_x(1)$ is looking promising (see Fig. 4.1) it turns out that the number of links close to where the point z_1 would be is very small even in the high density limit. Thus the rule Eq. (4.4) approximates the continuum rule Eq. (4.3) rather poorly because $\Omega_x(1)$ does not necessarily contain a point near the actual z_1 even for high ρ.

A potential alternative for $\Omega_x(1)$ is the following:

$$\Omega_x(1) = \{y \in \mathcal{C} \mid J^+(y) \cap (\mathcal{C} \setminus J^+(x)) = \emptyset\} \tag{4.7}$$

These are the points that are maximal in the subset of $\mathcal{C}$ that is not to the future of x. So it will cling to the lightcone of x from outside. The probability distribution for this set looks like in Fig. 4.1 flipped horizontally with z sitting at $(0, 0)$. It can be shown that with increasing density points near z will become more likely and thus that the approximation works well. Likewise all higher $\Omega_x(n)$ are no longer chosen to be minimal in $H_x^+(n)$ but to be maximal in $\mathcal{C} \setminus H_x^+(n)$:

$$\Omega_x(n) = \{y \in \mathcal{C} \mid J^+(y) \cap (\mathcal{C} \setminus H_x^+(n)) = \emptyset\} \tag{4.8}$$

Fig. 4.2b shows this modified algorithm in action and Fig. 4.2c shows the difference between the modified algorithm and the correct manifold result. One can see that the algorithm works well for most points but that with increasing number of paths the borders of the homotopy zones are detected

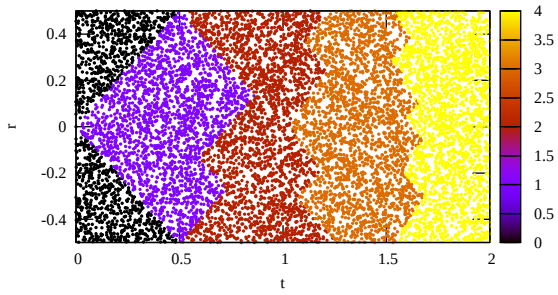

(a) $H_x(n)$ with $\Omega_x(n)$ obtained according to Eq. (4.6)

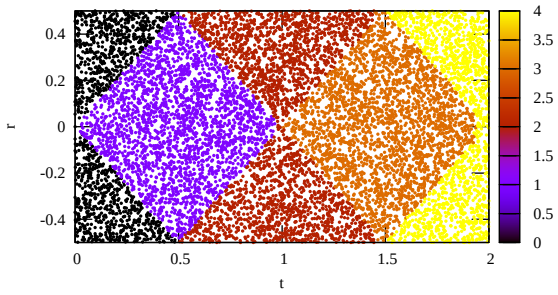

(b) $H_x(n)$ with $\Omega_x(n)$ obtained according to Eq. (4.8)

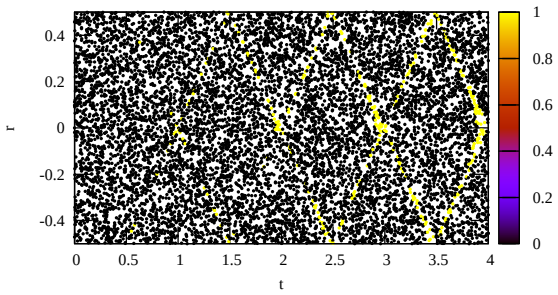

(c) Difference of A_H obtained from the modified algorithm and the correct manifold value

Figure 4.2: $(A_H)_{yx}$ for $x = (0, 0), y = (t, r)$ obtained by the causet algorithm for a sprinkling onto the cylinder with $L = 1, \langle N \rangle = 10000$. Two different choices of getting $\Omega_x(n)$ are shown.

less and less precisely. These errors would however only become observable if a particle coherently propagates much further than the circumference L.

The main flaw of the modified algorithm is that it must rely on the existence of enough elements spacelike to the perturbation source x to make the set $\Omega_x(1)$ a good approximation. If we were only to consider a sprinkling into a causal interval this algorithm will not be able to get the correct homotopy matrix entries for the minimal elements in that interval. Therefore strictly speaking the retarded propagator from x depends on elements that are spacelike to x. This certainly violates some sense of aesthetic.

4.3 Potential And Boundaries Of Generalizations

The algorithm has been introduced and explicitly discussed on the smooth cylinder manifold. So this alone would make applying the algorithm on a causal set a "cheat" as we put our knowledge that the set is a cylinder sprinkling into the process.

However it is easy to see that the algorithm applied to a $\mathbb{M}^2$ sprinkling would simply yield $(A_H)_{xy} = (A_C)_{xy}$ for all elements x where sufficient spacelike elements to form a good $\Omega_x(1)$ are available and with the possible exception of some y at the future boundary of the sprinkling area. The trivial and the cylinder topology are the two most important possible topologies in two dimensions. More exotic

ones like for example the "trousers" cause problems in defining even a continuum propagator and thus can safely be ignored for our purposes.

The presence of curvature will bend the lightcones and could therefore potentially mess with the concept of using the intersection points to determine the homotopy zones. However as long as one can find a coordinate system (t, x) in which the tangent vector ∂_t is always timelike and ∂_x is always spacelike then the algorithm is bound to work.

Putting all this together one might say that the algorithm works on all *relevant* two dimensional manifolds and we do not have to know precisely which one the sprinkling was done in to use it.

In dimensions higher than two the intersection of two lightcones will no longer be just a point but in general a $d-2$ dimensional hypersurface. Thus the trick to write the future of the intersection point z like in Eq. (4.3) will not be applicable in higher dimensions and therefore the whole procedure will not work. How to solve this problem is still an open question.

Chapter 5

Discrete D'Alembertian

5.1 Towards Replacing Differential Calculus

One of the most important tools in modern physics is differential calculus: Since its invention it has been used to formulate all major physical theories: Newtonian mechanics, electrodynamics, general relativity, quantum mechanics and quantum field theory. By giving up smooth manifolds the causal set approach also throws away this powerful tool. Maybe a theory can be built without notions of derivatives. However for the attempt to model "normal" field theory on a causal set it seems reasonable to investigate equivalents of differential operators thereon. One might think the first job is to find partial derivatives, as in the continuum they can be used to build all higher order operators. However partial derivatives imply a notion of tangent spaces which is also not developed yet on causal sets. Thus it has actually been easier to directly start out with the scalar d'Alembertian which on a Lorentzian manifold is given by

$$\Box = g^{\mu\nu} \nabla_\mu \partial_\nu \tag{5.1}$$

where ∇ denotes the covariant derivative with the torsion free metric connection.

In his seminal paper [13] Rafael Sorkin develops the concept of the discrete d'Alembertian for a causal set. Scalar fields on a causal set can be interpreted as vectors assigning a value to each point of the set. Thus an operator that acts linearly on fields must naturally be a matrix on that vector space.

For a two dimensional[1] causal set $\mathcal{C}$ and a function ϕ thereon the discrete d'Alembertian is given

[1] i.e. a sprinkling into a two dimensional manifold

by

$$
\begin{aligned}
(B\phi)_x &= \frac{4}{l_p^2}\left(-\frac{1}{2}\phi_x + \sum_{y\in\mathcal{C},y\prec x} f(n(y,x))\,\phi_y\right) \qquad (5.2)\\
&\text{with}\\
f(n) &= \begin{cases} 1 & \text{if } n=0\\ -2 & \text{if } n=1\\ 1 & \text{if } n=2\\ 0 & \text{else}\end{cases}\\
n(y,x) &= |\,\{z\in\mathcal{C}\mid y\prec z\prec x\}\,|.
\end{aligned}
$$

l_p denotes the discreteness scale given by $\rho^{-1/2}$. In this thesis a set $\{y\in\mathcal{C}\mid n(y,x)=n\}$ for some fixed n will be referred to as a "layer". The d'Alembertian is obtained by summing over the three closest layers in the past of x where closeness is understood in terms of cardinality of the intermediate causal interval.

It can be shown that for $\mathbb{M}^2$ sprinklings this operator yields

$$\langle (B\phi)_x\rangle = \Box\,\phi + \text{corrections} \qquad (5.3)$$

with corrections that die away as the sprinkling density grows. Here ϕ must be given as a continuous function on $\mathbb{M}^2$ and the causal set field is generated by taking $\phi_x=\phi(x)$. Thus for functions that vary slowly on the discreteness scale l_p and given an observation scale l_o such that $l_o\gg l_p$ the discrete B and the continuous $\Box$ are indistinguishable.

In the presence of curvature one finds [14]:

$$\langle (B\phi)_x\rangle = (\Box - \frac{1}{2}R)\,\phi + \text{corrections} \qquad (5.4)$$

Unfortunately this does not yet solve the problem. Although the expectation value tends to the right answer in the limit of high densities the fluctuations actually grow with the total number of elements. This does not have to be a problem: If the observation scale is large enough one might only be able to detect the averaged d'Alembertian over a region of the scale l_o^2 which might be a more well behaved quantity.

It is assumed however that big fluctuations are unfavourable and thus a less volatile operator was sought. The new candidate is [13]

$$
\begin{aligned}
(B_k\phi)_x &= \frac{4}{l_k^2}\left(-\frac{1}{2}\phi_x + \varepsilon\sum_{y\in\mathcal{C},y\prec x} f_\varepsilon(n(y,x))\,\phi_y\right) \qquad (5.5)\\
&\text{with}\\
f_\varepsilon(n) &= (1-\varepsilon)^n\left(1-\frac{2\,\varepsilon\,n}{1-\varepsilon}+\frac{\varepsilon^2\,n\,(n-1)}{2\,(1-\varepsilon)^2}\right)\\
\varepsilon &= (l_p/l_k)^2.
\end{aligned}
$$

Here a new, intermediate length scale l_k is introduced, called the *nonlocality* scale. A larger l_k increasingly damps the fluctuations however it also introduces new corrections. So in order to get both small fluctuations and small corrections l_k is supposed to be in between the discreteness scale l_p and our observation scale l_o. The discreteness scale is conjectured to be of the order of the Planck length. That would be $l_p \approx 10^{-35}$m. Given an energy scale of 1 TeV the current observation scale is roughly $l_o = 10^{-16}$m. So a priori there is plenty of "space" for the new intermediate scale. Nevertheless we should keep in mind that the introduction of a new physical length scale is a strong assumption that needs to be justified at some point.

The operator in Eq. (5.2) is referred to as the *local* discrete d'Alembertian whereas Eq. (5.5) is called *nonlocal*. In the non-local version the way the layers contribute to the d'Alembertian is "smeared out" over more layers (see Fig. 5.1a). In the limit $\varepsilon \to 1$ both versions coincide.

Fig. 5.1b illustrates how the points in a $\mathbb{M}^2$ sprinkling contribute to the overall value of the d'Alembertian.

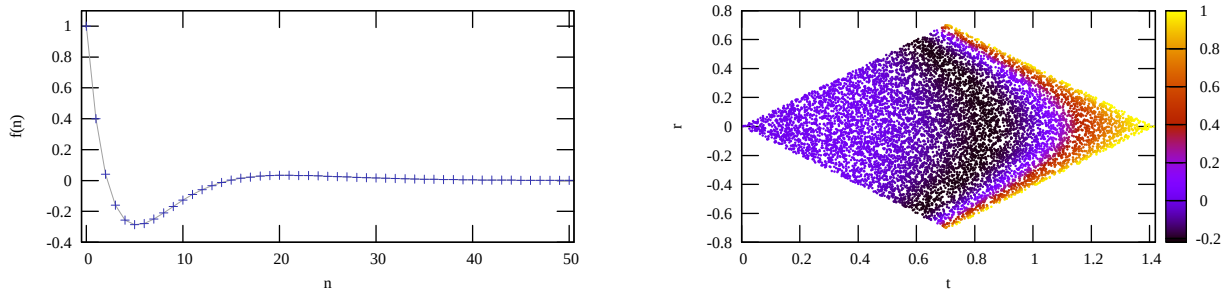

(a) $f_\varepsilon(n)$ for $\varepsilon = 0.2$

(b) $f_\varepsilon(n(y,x))$ on a sprinkling in $\mathbb{M}^2$ with $x = (\sqrt{2}, 0), y = (t, r), \varepsilon \approx 8.2 \cdot 10^{-4}$

Figure 5.1: The non-local d'Alembertian

5.2 Physical Length Scales

Computing the discrete d'Alembertian of a constant function enables one to study the scalar curvature of a given set. This relies on a sensitive interplay of various different physical length scales: The discreteness scale l_p, the non-locality scale l_k, the curvature scale $l_c = |R|^{-1/2}$ and the length scale associated with the volume of the sprinkling region Ω: $l_v = V(\Omega)^{1/2}$. We need $l_p \ll l_k$ so that the averaging effect of the non-local d'Alembertian kicks in. At the same time we need l_p and $l_k \ll l_c$ so that the underlying discrete network is fine enough to capture all the relevant information about the spacetime curvature. Finally we need $l_c \lesssim l_v$ so that the sampled spacetime volume is at least big enough to make the deviation of curved space from flat space detectable. For everything to work out just fine we want

$$l_p \ll l_k \ll l_c \lesssim l_v. \tag{5.6}$$

De Sitter space offers a nice test object to study this hierarchy with the aid of numerical simulations. We will work in two dimensions and in conformally flat coordinates (cf. Sec. 2.4.4). In these coordinates the scalar curvature is $R = 2/\alpha^2$ (cf. Eq. (2.22)) and the volume of a causal interval bounded by the points $x = (t_0, 0)$, $y = (t_1, 0)$, $t_1 > t_0$ is (cf. Eq. (2.21))

$$V(x,y) = 2\alpha^2 \ln\left(\frac{(t_0+t_1)^2}{4\,t_0\,t_1}\right). \tag{5.7}$$

So for a sprinkling with an expected number of elements $N = \rho \cdot V(x,y)$ into this interval we find

$$\begin{aligned} l_p &= (V(x,y)/N)^{1/2} &&= \alpha\, N^{-1/2} \left(2\ln\left(\tfrac{(t_0+t_1)^2}{4\,t_0\,t_1}\right)\right)^{1/2} \\ l_c &= |R|^{-1/2} &&= \alpha\sqrt{2} \\ l_v &= V(x,y)^{1/2} &&= \alpha \left(2\ln\left(\tfrac{(t_0+t_1)^2}{4\,t_0\,t_1}\right)\right)^{1/2}. \end{aligned} \tag{5.8}$$

For a well working d'Alembertian we would like $N \gg \ln\left(\frac{(t_0+t_1)^2}{4\,t_0\,t_1}\right) \gg 1$ and l_k must be chosen appropriately.

5.3 Numerical Preliminaries

There are some issues concerning the numerical evaluation of the discrete d'Alembertian on a sprinkling which shall be mentioned before proceeding to discussing the actual results.

First there is the finiteness of the sprinkling interval. According to Eqns. (5.2) and (5.5) one is supposed to sum over all $\{y \in \mathcal{C} \mid y \prec x\}$ so surely the shape of the sprinkling interval somehow influences the resulting value of the d'Alembertian. Analytical calculations for the expectation value usually assume an unbounded sprinkling area which can naturally not be realized on a computer. Let $N_{\mathrm{card}}(x,n)$ denote the cardinality of the n-th layer, i.e. the number of elements y such that $n(y,x) = n$ i.e.

$$N_{\mathrm{card}}(x,n) = |\{y \in \mathcal{C} \mid n(y,x) = n\}|. \tag{5.9}$$

On full Minkowski space $\langle N_{\mathrm{card}}(x,n)\rangle$ is infinite. To get reasonable results for the d'Alembertian on finite sprinkling intervals these intervals must be at least so big that the cut-off has about the same effect on every layer.

Fortunately geometry comes to the rescue in the de Sitter 2d case case. The expectation value of N_{card} is finite even for unbounded regions:

$$\langle N_{\mathrm{card}}(x,n)\rangle = \int_{y\in J^-(x)} d^2y\ \sqrt{-g}\ \rho \frac{(\rho V(y,x))^n}{n!}\ \exp(-\rho\, V(y,x)) \tag{5.10}$$

Plugging in the suitable metric determinant and volume formula and parametrising the past $J^-(x)$ of $x = (t_1, 0)$ appropriately this integral reads

$$\langle N_{\mathrm{card}}(x,n)\rangle = \int_{-\infty}^{t_1} dt \int_{-(t_1-t)}^{+(t_1-t)} dr\ \frac{\rho\,\alpha^2}{t^2}\ \frac{\left(2\,\rho\,\alpha^2\ \ln\left(\frac{(t_1+t)^2-r^2}{4\,t_1\,t}\right)\right)^n}{n!}\ \left(\frac{(t_1+t)^2-r^2}{4\,t_1\,t}\right)^{-2\rho\alpha^2} \tag{5.11}$$

For general n this integral is quite intractable. For the special case $n = 0$ the finiteness can be shown by an upper bound estimation. If the number $N_{\mathrm{card}}(x, 0)$ for any x is finite so will be all higher $N_{\mathrm{card}}(x, n > 0)$ for any given n. If x has only a limited number of links in the past and each of these again has only a limited number of links in the past then $N_{\mathrm{card}}(x, 1)$ is bound to be finite as well and so on and so forth. This means there is an intrinsic cut-off in de Sitter 2d which suppresses to some extent the difference between an infinite and a large enough finite sprinkling region. The necessary interval size can be estimated by evaluating Eq. (5.11) numerically.

Then there is the scale factor α introduced by the embedding of de Sitter 2d into $\mathbb{M}^3$. For the d'Alembertian of the constant function $\phi = 1$ we expect $(B\,\phi)_x = -\alpha^{-2}$ so at first glance it seems like a good test to search for this particular dependence for varying α. However a closer look reveals that α is merely a superficial scale having no real influence on the structure of the sprinkling. This can be seen in various places:

For example all the length scales in Eq. (5.8) are proportional to α. Thus α has no influence on their relative size. The integral Eq. (5.11) is invariant under rescaling $\alpha \to \lambda\alpha$ and $\rho \to \rho\lambda^{-2}$. If one considers a sprinkling into a given causal interval $I(x, y)$ with a given number of expected elements N then one will find $\rho = N/V(x, y) = (\ldots) \cdot \alpha^{-2}$. So rescaling α automatically rescales ρ in a way that leaves $\rho\,\alpha^2$ invariant and thus the value of Eq. (5.11). The invariance becomes most obvious in the sprinkling map Eq. (2.20) which shows no dependence on α whatsoever. Due to conformal flatness also the causal relations of two given points are not influenced by α. Given this not only is the integral Eq. (5.11) but in fact the whole structure of the sprinkled set independent of α.

Thus if we parametrize l_k relative to α e.g. $l_k = \alpha\, l'_k$ like the other physically relevant scales (Eq. (5.8)) then rescaling α will leave invariant the causal structure of the set as well as the parameter $\varepsilon = (l_p/l_k)^2$ thus making the prefactor $\frac{4}{l^2_{(p,k)}}$ in Eqns. (5.2) and (5.5) the only remaining dependence of B and B_k on α which leaves exactly the α^{-2} proportionality that one would have expected.

So we can simply fix α to some arbitrary value and do not have to collect simulation data for different values which of course saves a lot of otherwise uselessly wasted computation effort.

Another simplification becomes possible when computing the d'Alembertian of the constant function $\phi = 1$. Then Eq. (5.5) can be written as

$$\begin{aligned}(B(\phi = 1))_x &= \frac{4}{l_k^2}\left(-\frac{1}{2} + \varepsilon \sum_{y \in \mathcal{C}, y \prec x} f(n(y, x))\right) \\ &= \frac{4}{l_k^2}\left(-\frac{1}{2} + \varepsilon \sum_{n=0}^{\infty} f(n)\, N_{\mathrm{card}}(x, n)\right)\end{aligned}$$

and

$$\langle (B(\phi = 1))_x \rangle = \frac{4}{l_k^2}\left(-\frac{1}{2} + \varepsilon \sum_{n=0}^{\infty} f(n)\, \langle N_{\mathrm{card}}(x, n) \rangle\right). \tag{5.12}$$

Thus for the computation of the expectation value one can first gather data about the expectation values of $N_{\mathrm{card}}(x, n)$ without having to specify a non-locality scale l_k. Then one can use this distribution to evaluate the expectation value of B_k for arbitrary l_k without further simulations.

5.4 Simulation Results

The aim of the simulations is to investigate the discrete d'Alembertian of the constant function $\phi = 1$ on sprinklings into de Sitter 2d in order to study the scalar curvature. Both mean and fluctuations of the d'Alembertian shall be examined. The sprinklings are created on a causal interval $I(x_0, x_1)$ between the points $x_0 = (t_0, 0)$ and $x_1 = (t_1, 0)$ and the d'Alembertian evaluation point x is always chosen to be the futuremost point in the sprinkling. Given the strict definition of $\langle B\phi \rangle_x$ the element x should have been fixed to always sit exactly at the tip of the interval. But numerics indicate that the results are not significantly affected by this.

The first step in the simulations is to gain data about the distribution of $N_{\mathrm{card}}(x, n)$. Figs. 5.2a and 5.2b illustrate data of two major simulation sets. In both cases it was chosen $t_0 = -150, t_1 = -1, \alpha = 1$. t_0 has been chosen very small in order to reach the regime of the intrinsic cut-off for at least the first couple of layers. This has been verified via numerical integration. The simulations differ in the total number of expected elements $\langle N \rangle$ which has been chosen to be 1000 and 10000 respectively in order to study the influence of that quantity.

Figs. 5.2c and 5.2d show a close-up on the first layers and additionally the results of numerical integration where one must unfortunately conclude the numerical integration for $\langle N \rangle = 1000$ did not yield useable results.

This data can now be used to compute the discrete d'Alembertian for any non-locality scale according to Eq. (5.12). Fig. 5.3a and 5.3b show the mean value and the standard error for varying l_k, Fig. 5.3c shows a combined plot. For $\alpha = 1$ and the constant function $\phi = 1$ one would expect $\langle (B_k \phi)_x \rangle = -R/2 = -1$. Clearly this is not the result one gets in the regime for larger l_k where the fluctuations are small. With increasing l_k the mean value drifts further away from $B_k = -1$ and one can see in Fig. 5.3a and 5.3c that after l_k passes the curvature scale $l_c = R^{-1/2} \approx 0.71$ the discrepancy becomes even worse. As the combined plot shows both data series coincide in the regime of small error. So one can deduce that the sprinkling size is unlikely to have an influence on the observed deviations. For $l_k \to l_p$ both plots give hope that the mean might tend towards $B_k = -1$ as predicted by theory. However the fluctuations become so large that the limit of the local d'Alembertian seems to be numerically intractable.

Fig. 5.3d shows the standard deviation of single evaluations for both data series. One can see that for the local versions the fluctuations grow with $\langle N \rangle$ whereas for the non-local version the fluctuations are clearly damped with increasing l_k and also that given a fixed l_k the fluctuations become smaller

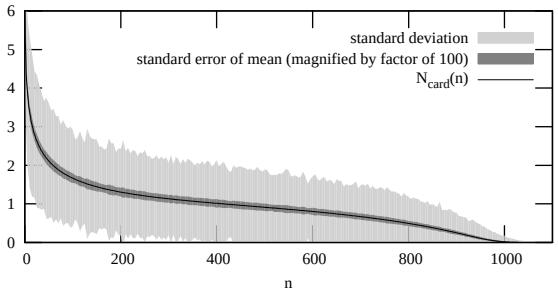

(a) $\langle N \rangle = 1000$, averaged over 1.00 million runs. $\langle N_{\mathrm{card}}(n=0) \rangle \approx 6.19$.

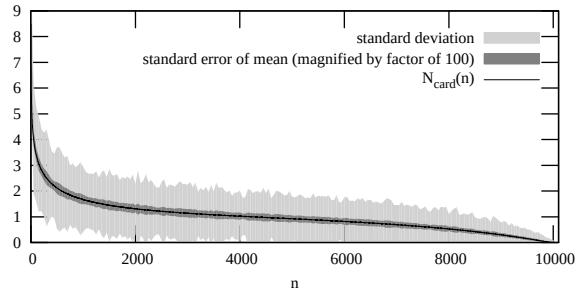

(b) $\langle N \rangle = 10,000$, averaged over 0.48 million runs. $\langle N_{\mathrm{card}}(n=0) \rangle \approx 8.49$.

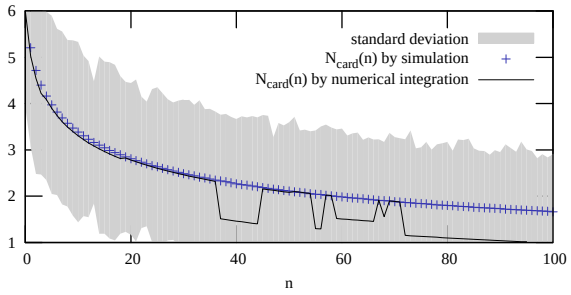

(c) Closeup of $\langle N \rangle = 1000$ with numerical integration.

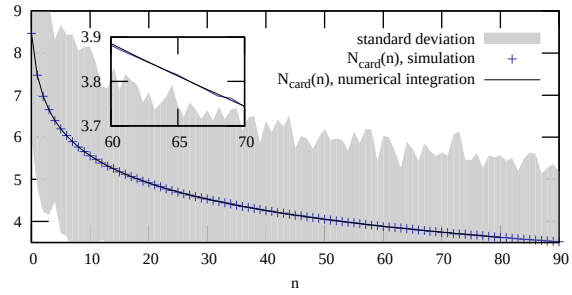

(d) Closeup of $\langle N \rangle = 10,000$ with numerical integration. The inset shows an extreme closeup on which the small but existent fluctuations of the simulation data can be seen.

Figure 5.2: $\langle N_{\mathrm{card}}(x,n) \rangle$ on de Sitter 2d for the topmost element x in a causal interval between $(-150,0),(-1,0)$ for $\langle N \rangle$ expected elements, obtained by simulation and numerical integration of Eq. (5.11). The shown standard deviations are estimated from the standard deviations of bundles of 10,000 runs. For $\langle N \rangle = 1000$ numerical integration appears to be unstable.

with increasing $\langle N \rangle$.

The relation between l_k and the fluctuations can be understood when looking at the high relative standard deviation of the layer cardinality data $N_{\mathrm{card}}(n,x)$ in Fig. 5.2. Given a high non-locality scale the data is averaged over many layers and thus the fluctuations become suppressed. For small l_k even the hardly noticeable noise in the data averaged over many runs (cf. inset in Fig. 5.2d) is enough to severely disturb the mean value.

To still get a glimpse of how the d'Alembertian behaves in the limit $l_k \to l_p$ one can try to fall back on numerically integrated layer data. For the $\langle N \rangle = 10000$ case seemingly reasonable results up to $n \approx 80$ were obtained (see Fig. 5.2b) and so it is worth a try to plug these into the d'Alembertian computation. The outcome is shown in Fig. 5.3b. For large l_k the weight function $f(n)$ lives long enough to "see" that layer data is only available up to $n = 80$ and thus the results are invalid. Only when this boundary becomes invisible to $f(n)$ one can see reasonable values that are indeed very close to the expected result $B_k = -1$. For $l_k \to l_p$ even the precision of this data is no longer good enough and so the mean diverges at this "wall". It is hard to estimate the error for this dataset but the mean

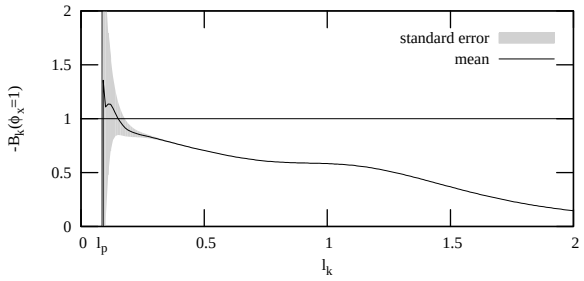

(a) -$\langle B_k(\phi = 1)_x\rangle$ for $\langle N\rangle = 1000$, averaged over 1.00 million runs. $l_p \approx 0.085$.

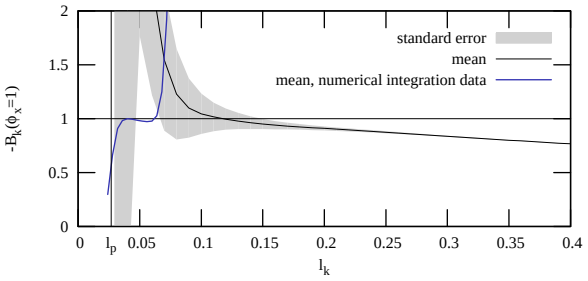

(b) -$\langle B_k(\phi = 1)_x\rangle$ for $\langle N\rangle = 10000$, averaged over 0.48 million runs and data from numerical integration. $l_p \approx 0.027$.

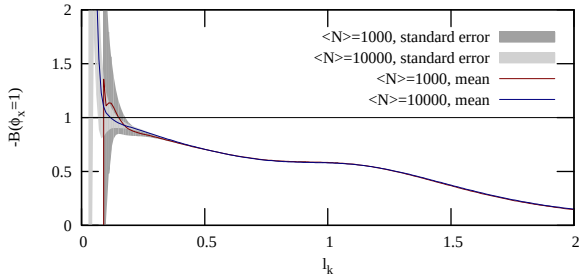

(c) Combined plot of $\langle N\rangle = 1000$ and $\langle N\rangle = 10000$.

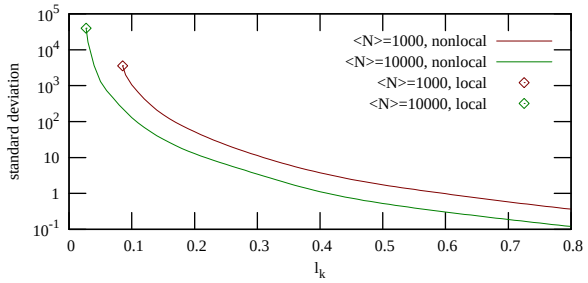

(d) Estimated standard deviation of a single evaluation for local and non-local d'Alembertian

Figure 5.3: $\langle B_k(\phi = 1)_x\rangle$ on de Sitter 2d for the topmost element x in a causal interval between $(-150, 0), (-1, 0)$ for $\langle N\rangle$ expected elements and varying non-locality scale l_k, obtained by simulation and numerical integration. The shown standard deviations are estimated from the standard deviations of bundles of 10,000 runs.

is nevertheless a good indicator that the d'Alembertian might indeed approach $B_k = -1$ in the limit of small non-locality.

This presented simulation data has demonstrated that $l_p \ll l_k$ is necessary for reasonable small fluctuations and has given us a hunch that $l_k \ll l_c$ might be helpful to keep corrections small. However one would want this relation to be established more solidly and furthermore the interplay of l_c and l_v has not been seen yet. To this end another set of simulations is discussed here that can give insight in these two relations.

The setup will be to compare sprinklings into intervals of varying volume to study what happens when $l_c \gg l_v$. In this limit one would expect a transition to Minkowskian behaviour as the curvature should become less and less detectable. The sprinkling intervals are again chosen to be causal intervals between $x_0 = (t_0, 0)$ and $x_1 = (t_1, 0)$ with $t_0 = -150$ fixed and varying $t_1 \in [-145, -1]$. As the ratio of the volumes $V(x_0, x_1|t_1 = -1)/V(x_0, x_1|t_1 = -145) = \mathcal{O}(10^4)$ it seems unsuitable to keep the sprinkling density ρ fixed. Instead the number of expected elements $\langle N\rangle = \rho \cdot V$ will be kept constant. This however induces another difficulty: The different causal sets will have very different discreteness

scales.

A priori a causal set has no notion of fundamental length scale whatsoever. All "higher" scales like curvature and volume scale are measured only in terms of the only natural available measure for size: The number of elements. We like to associate a fundamental length scale to the distance of two neighbouring points in order to make the comparison with manifolds possible. But when one wants to compare the properties of two causal sets one should ensure that the associated fundamental length scales are comparable.

As the transition of the de Sitter sprinklings towards Minkowski space is to be investigated a Minkowski sprinkling with the same discreteness scale will serve as reference. By rescaling the coordinate system $(t, x) \to (\lambda \cdot t, \lambda \cdot x)$ a Minkowski sprinkling can be resized to any desired discreteness scale. Under such a rescaling the non-locality scale transforms like $l_k \to \lambda \cdot l_k$ and the d'Alembertian $B_k \to \lambda^{-2} B_k$.

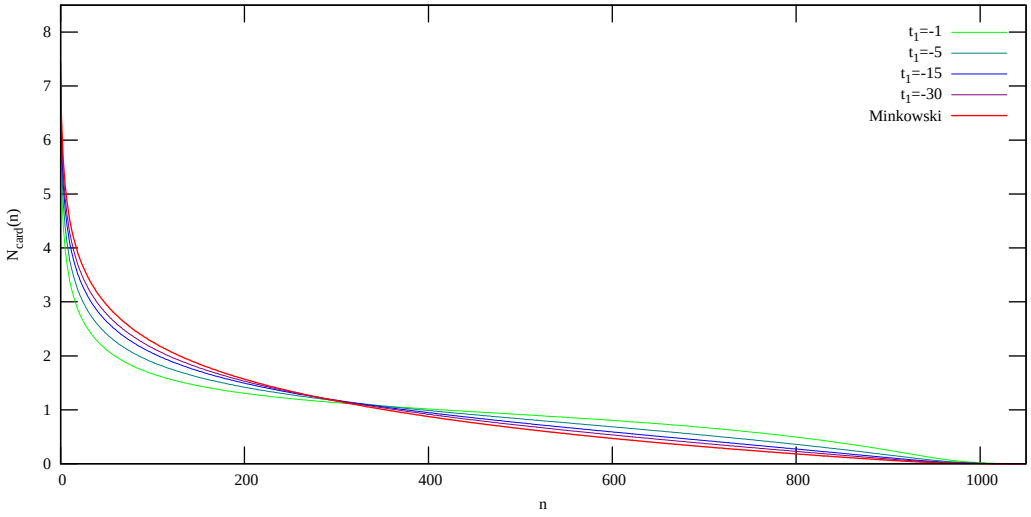

Figure 5.4: $\langle N_{\text{card}} \rangle$ of the topmost element of a sprinkling into causal intervals between $(t_0, 0)$ and $(t_1, 0)$ on de Sitter 2d compared to data from a Minkowski sprinkling with same number of elements. For $t_1 \to t_0$ one can see a transition from de Sitter towards Minkowski.

The transition of de Sitter into Minkowski already becomes visible when looking at the cardinality of the layers (see Fig. 5.4): The closer t_0 and t_1 become the weaker becomes the variation of the metric determinant throughout the interval and thus the more de Sitter space looks like $\mathbb{M}^2$. However the de Sitter layer data already looks quite indistinguishable for $t_1 \lesssim -80$ whereas the full d'Alembertian is still able to separate de Sitter from Minkowski for $t_1 \gtrsim -120$ as we shall see.

Fig. 5.5 shows the results of $\langle B_k \rangle$ for different t_1. For $t_1 = -145$ one has $V(x_0, x_1) \approx 5.75 \cdot 10^{-4}$, $l_p \approx 7.58 \cdot 10^{-4}$ and the ratio $l_c / l_v \approx 30$. The smallest fluctuations in the causal structure of the set become amplified with a prefactor of $4 \cdot l_p^{-2} \approx \mathcal{O}(10^{10})$ (cf. Eq. (5.5)) which causes a very big fluctuation scale and thus makes it impossible to detect a curvature that is so small in comparison. For $t_1 = -120$ the two sets are already distinguishable within the accuracy of errorbars and for $t_1 = -80$

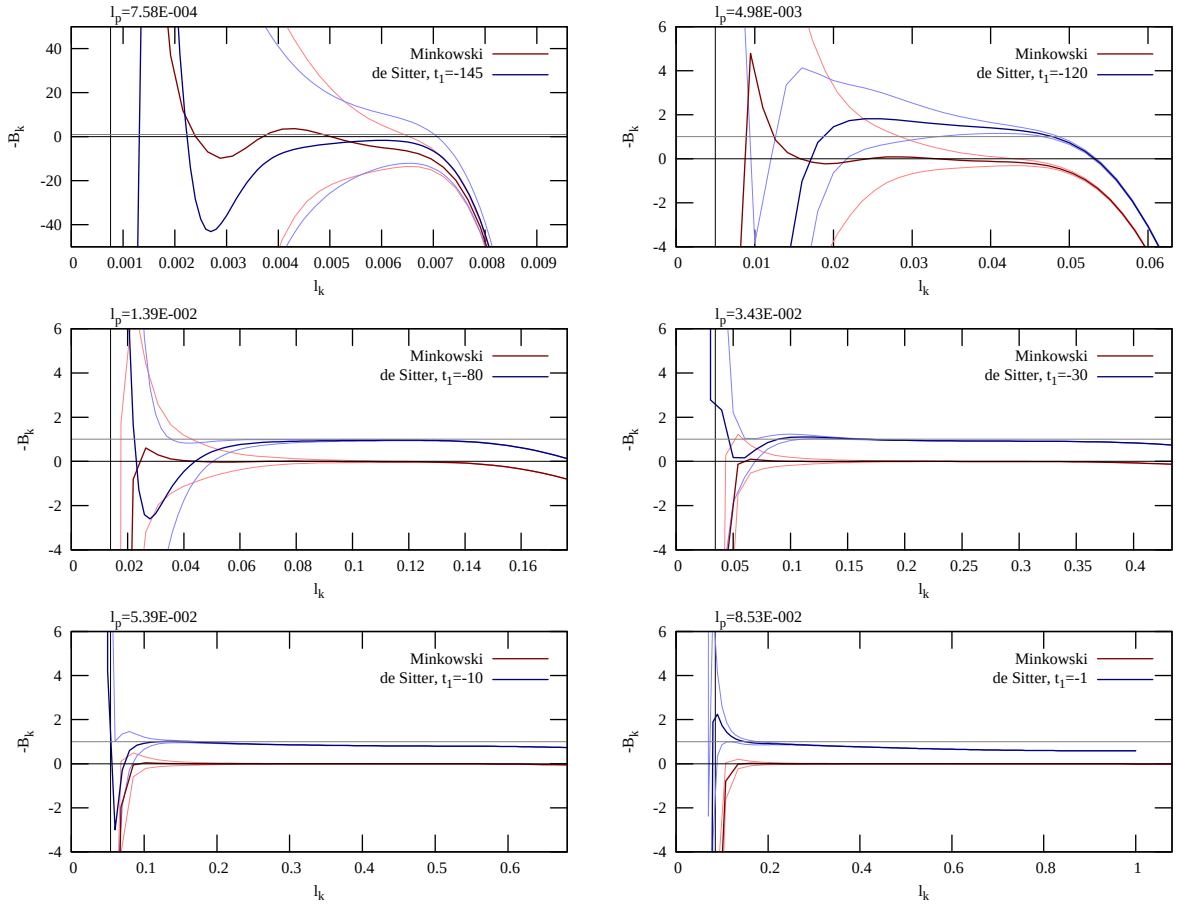

Figure 5.5: Discrete d'Alembertian of $\phi = 1$ of sprinklings into causal intervals $I((t_0, 0), (t_1, 0))$ of varying size on de Sitter 2d. $\langle N \rangle = 1000$, $\alpha = 1$, $t_0 = -150$, t_1 is given in the key of each plot. For comparison the average of the same $\mathbb{M}^2$ data but scaled to the correct volume and density is shown. Lighter lines indicate standard errors. The horizontal grey line shows $R/2 = 1$. Data is averaged over 1.00 million runs.

there is no doubt left that one sprinkling is flat and the other one is curved. Although at $t_1 = -80$ the ratio $l_c/l_v \approx 1.6$ this already seems to be enough to make the curvature detectable. Possibly the intrinsic cut-off of de Sitter geometry hinders the d'Alembertian from seeing the full causal set and thus it is not that important how big the volume of the whole set is after all.

As there is no curvature scale on Minkowski the discrepancy of the Minkowski d'Alembertian for large l_k must be due to the finiteness of the sprinkling interval. For $t_1 = -145, -120, -80$ one can see that the de Sitter data starts to diverge in the same way and thus probably for the same reason. For $t_1 = -10, -1$ however the de Sitter data starts to leave the ideal level earlier and one can conclude that this must be due to corrections in orders of l_k/l_c. In all plots $l_c = R^{-2} \approx 0.707$ but only in the plots for big t_1 l_k becomes comparably large. Unfortunately only very little is known about the exact form of these corrections. They are expected to be of the general form $l_k^{2(n+m-1)} \Box^m R^n$. In any case one can state that $l_k \ll l_c$ keeps corrections down.

Chapter 6

Action

6.1 Winnowing Wheat From Chaff[1]

For very large N the set of all causal sets with cardinality N will be dominated by sets that allow no manifold interpretation whatsoever [15]. It is therefore of vital importance for the causal set programme to find the ones that do.

To this end a quantity is looked for that can somehow distinguish between an arbitrary and a manifold like causal set. In the causal set context such a quantity is called *action* because it is expected to act analogous to the action in quantum mechanics: There the principle of least action isolates the classical path from the huge spectrum of all paths. In a similar fashion it is hoped the causal set action will find the sets that have a continuous manifold approximation and are classical solutions of Einstein's equations to boot (see [14] for a discussion of this).

In [14] a candidate for two dimensions is proposed:

$$
\begin{aligned}
S(\mathcal{C}) &= \sum_{x\in\mathcal{C}} \left(-\frac{1}{2} + \sum_{y\in\mathcal{C}\cap J^-(x)} f(n(y,x)) \right) \qquad (6.1)\\
&\text{with}\\
J^-(x) &= \{y \in \mathcal{C} \mid y \prec x\}\\
n(y,x) &= |\{z \in \mathcal{C} \mid y \prec z \prec x\}|\\
f(n) &= \begin{cases} 1 & \text{if } n = 0 \\ -2 & \text{if } n = 1 \\ 1 & \text{if } n = 2 \\ 0 & \text{else} \end{cases}
\end{aligned}
$$

The action consists of two components: The part that only depends on the sum over x is called the *local* contribution whereas the part that depends on the sum over x and y will be referred to as *bilocal*.

Up to a prefactor this is simply adding up the local discrete d'Alembertian of $\phi = 1$ evaluated at

[1] This section is named after a talk that Joe Henson gave at the *Causets at DIAS II* conference in December '09

each point of the set:

$$S(\mathcal{C}) \;=\; \frac{l_p^2}{4}\sum_{x\in\mathcal{C}}\left(B(\phi=1)\right)_x \tag{6.2}$$

The expectation value for the action of a causal set sprinkled into a region Ω of a two-dimensional Lorentzian manifold is

$$\begin{aligned}\langle S\rangle(\Omega) &= \int_\Omega d^2x\,\sqrt{-g(x)}\,\rho\left(-\frac{1}{2}+\int_{\Omega\cap J^-(x)} d^2y\,\sqrt{-g(y)}\,\rho\sum_{n=0}^{\infty}\mathrm{P}(n(y,x)=n)\,f(n)\right)\\ &= -\frac{1}{2}\rho\,V(\Omega)+\int_\Omega d^2x\int_{\Omega\cap J^-(x)} d^2y\,\sqrt{g(x)g(y)}\,\rho^2\,p(\rho\,V(y,x)) \qquad (6.3)\\ \text{with } p(x) &= (1-2x+x^2/2)\,\exp(-x).\end{aligned}$$

Sometimes it seems a little more convenient to change the order of integration of x and y and one might use

$$\int_\Omega d^2x\int_{\Omega\cap J^-(x)} d^2y\,F(x,y)=\int_\Omega d^2y\int_{\Omega\cap J^+(y)} d^2x\,F(x,y) \tag{6.4}$$

for some integrand $F(x,y)$. Naturally the proposition of a candidate must be followed by evaluating its suitability. This is what the following chapter is about. The expectation value for selected sprinkling regions shall be investigated to gain a rough picture of the behaviour of S.

6.2 Causal Intervals On $\mathbb{M}^2$

For a causal interval on two dimensional Minkowski space the expectation value of the action can be computed analytically. Just like in Sec. 2.4.1 first Poincaré symmetry is used to pick coordinates in which the interval is bounded by $(0,0)$ and $(0,T)$ in Cartesian coordinates and then one switches to lightcone coordinates $(u,v)\in\Omega=[0,a=T/\sqrt{(2)}]^2$ (cf. Eq. (2.5)). The volume of the causal interval with edge lengths Δu and Δv is $V(I((0,0),(\Delta u,\Delta v)))=\Delta u\cdot\Delta v$. Plugging all this into Eq. (6.3) one finds

$$\begin{aligned}\langle S\rangle(\Omega) &= -\frac{\rho\,a^2}{2}+\int_0^a du_x\int_0^a dv_x\int_0^{u_x} du_y\int_0^{v_x} dv_y\,\rho^2\,p(\rho\,\Delta u\,\Delta v)\\ \text{with}\quad & \Delta u=u_x-u_y,\ \Delta v=v_x-v_y\\ &= -\frac{\rho\,a^2}{2}+\int_0^a du_x\int_0^a dv_x\int_0^{u_x} d\Delta u\int_0^{v_x} d\Delta v\,\rho^2\,p(\rho\,\Delta u\,\Delta v)\\ &= -\frac{\rho\,a^2}{2}+\int_0^a du_x\int_0^a dv_x\left[[\text{integrand 1}]_{\Delta v=0}^{\Delta v=v_x}\right]_{\Delta u=0}^{\Delta u=u_x}\\ \text{with}\quad & \text{integrand 1}=-\frac{\rho}{2}\,(1-\rho\,\Delta u\,\Delta v)\,\exp(-\rho\,\Delta u\,\Delta v)\\ & [g(\xi)]_{\xi=\beta}^{\xi=\alpha}=g(\alpha)-g(\beta).\end{aligned}$$

Hence

$$\langle S\rangle(\Omega) \;=\; -\frac{1}{2}(1-\exp(-\rho\,a^2)). \tag{6.5}$$

The edge length a depends on the choice of coordinates. The value $a^2 = V(\Omega)$ however is Lorentz invariant. So one finds for arbitrary causal intervals on Minkowski 2d:

$$\langle S\rangle(\Omega) = -\frac{1}{2}(1 - \exp(-\rho\, V(\Omega))) \tag{6.6}$$

Consider now splitting up the interval Ω into four smaller intervals Ω_i according to Fig. 6.1a. When computing the expected action one can split up the contributions into the actions of the four sub intervals plus the bilocal contributions when x and y are lying in two different intervals. Let $\langle S_2\rangle(\Omega_i, \Omega_j)$ denote the expected bilocal contributions from all $x \in \Omega_i$ and all $y \in \Omega_j$. Then one gets

$$\langle S\rangle(\Omega) = \sum_{i=1}^{4}\langle S\rangle(\Omega_i) + \langle S_2\rangle(\Omega_2,\Omega_1) + \langle S_2\rangle(\Omega_3,\Omega_1) + \langle S_2\rangle(\Omega_4,\Omega_1) + \langle S_2\rangle(\Omega_4,\Omega_2) + \langle S_2\rangle(\Omega_4,\Omega_3) \tag{6.7}$$

The bilocal summands can be computed using the same integral as in Eq. (6.5) and adjusting the

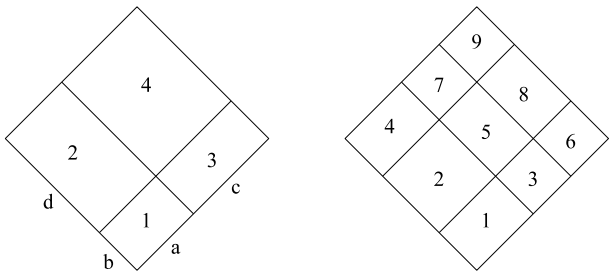

(a) (b)

Figure 6.1: Splitting up a causal interval on Minkowski 2d to compute the action

boundaries (and naturally dropping the local component). This yields

$$\begin{aligned}
\langle S_2\rangle(\Omega_2,\Omega_1) &= \int_0^a du_x \int_b^{b+d} dv_x \int_0^{u_x} du_y \int_0^b dv_y\, \rho^2\, p(\rho\,\Delta u\,\Delta v) \\
&= \int_0^a du_x \int_b^{b+d} dv_x \left[\text{[integrand 1]}_{\Delta v = v_x - b}^{\Delta v = v_x}\right]_{\Delta u = 0}^{\Delta u = u_x} \\
&= \frac{1}{2}(1 - \exp(-a\,b\,\rho) - \exp(-a\,d\,\rho) + \exp(-a\,(b+d)\,\rho)) \qquad (6.8) \\
\langle S_2\rangle(\Omega_4,\Omega_1) &= \int_a^{a+c} du_x \int_b^{b+d} dv_x \int_0^a du_y \int_0^b dv_y\, \rho^2\, p(\rho\,\Delta u\,\Delta v) \\
&= \int_a^{a+c} du_x \int_b^{b+d} dv_x \left[\text{[integrand 1]}_{\Delta v = v_x - b}^{\Delta v = v_x}\right]_{\Delta u = u_x - a}^{\Delta u = u_x} \\
&= -\frac{1}{2}\,(1 - \exp(-(a+c)\,(b+d)\,\rho) \\
&\quad + \exp(-a\,(b+d)\,\rho) + \exp(-c\,(b+d)\,\rho)) + \exp(-(a+c)\,b\,\rho) + \exp(-(a+c)\,d\,\rho) \\
&\quad - \exp(-a\,b\,\rho) - \exp(-a\,d\,\rho) - \exp(-c\,b\,\rho) - \exp(-c\,d\,\rho)) \qquad (6.9)
\end{aligned}$$

The contributions for the combinations (3,1),(4,2) and (4,3) can be obtained from $\langle S_2\rangle(\Omega_2,\Omega_1)$ by swapping the appropriate parameters. Putting together all parts of Eq. (6.7) one exactly recovers Eq. (6.6).

Now one might want to continue this game and split up the interval even further like in Fig. 6.1b. To compute the action one must again sum up all local and bilocal terms. We already know the local contributions and the bilocal ones from two intervals that share either an edge or a vertex (cf. $\langle S_2\rangle(\Omega_2, \Omega_1)$ and $\langle S_2\rangle(\Omega_4, \Omega_1)$ in Fig. 6.1a). Now one must work out the remaining ones like (4,1),(7,1) and (9,1) in Fig. 6.1b. It turns out they only consist of exponentials that quickly die away as the density is raised. All that one is left with in this limit is $-1/2$ for every sub interval, $1/2$ for every edge between two sub intervals and $-1/2$ for every two sub intervals that share a vertex. One could write

$$\langle S\rangle = -\frac{1}{2}(\mathbf{F} - \mathbf{E} + \mathbf{V}) \tag{6.10}$$

where $\mathbf{F}$ denotes the number of *faces* i.e. intervals, $\mathbf{E}$ the number of shared edges and $\mathbf{V}$ the number of shared vertices. This strongly reminds one of the computation of the Euler characteristic of triangulations of two dimensional manifolds and motivates the question: Is the expected action (to some extent) a topological constant? It is obvious that the formula can be applied to arbitrary areas constructed from tilings of causal intervals as long as each interval is large enough to neglect the corrections and as long as the created areas are causally convex meaning that for any two points $y \prec x$ picked therefrom their causal interval $I(y, x)$ is also wholly contained in the area. This is required to make the used formula for the intermediate volume $V = \Delta u \Delta v$ valid. It is not hard to verify that each of these constructions will yield an expected action $\langle S\rangle = -1/2$ in the limit.

So for example the region sketched in Fig. 6.2a will give $\langle S\rangle = -1/2$ in the limit of high density but the region in Fig. 6.2b will not.

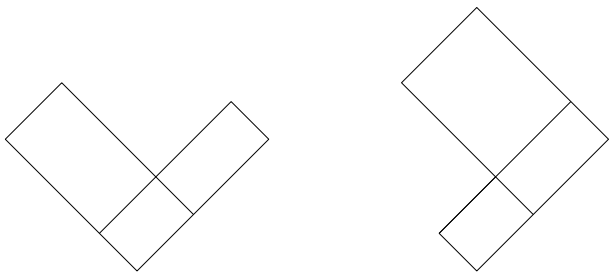

(a) causally convex (b) not causally convex

Figure 6.2: Different regions constructed from causal intervals on $\mathbb{M}^2$

6.3 Causal Intervals On The Cylinder

Naively applying formula Eq. (6.10) to a causal interval on a cylinder with circumference L and height T with $L \leq T \leq 2L$ one might come up with a subdivision as sketched in Fig. 6.3a. Taking into account the topological identification one finds $\mathbf{F} = 8, \mathbf{E} = 12, \mathbf{V} = 4$ thus yielding a predicted high-density expectation value of $\langle S\rangle = 0$. Performing corresponding simulations this is what one will

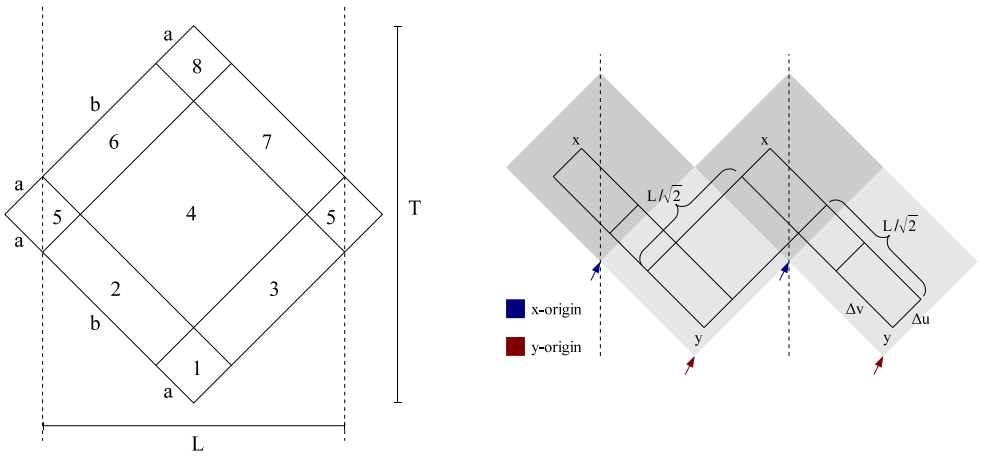

(a) $L \leq T \leq 2L$ (b) How to compute $V(y, x \mid x \in H_y(2))$.

Figure 6.3: Computing the action on a cylinder

actually find. However we have not shown yet that formula Eq. (6.10) is applicable to the cylinder after all. The segmentation of the causal interval in Fig. 6.3a has been chosen such that formula Eq. (6.6) for the faces and formulas Eq. (6.8) and (6.9) for the bilocal contributions of two intervals that share an edge or a vertex can still be applied as the cylinder topology does not yet affect these cases. But the computation of contributions like (5,1),(6,1) and (8,1) differs from the Minkowski setup because alternative paths between two points that go around the cylinder are now accessible and thus the intermediate causal volume $V(y, x)$ is altered.

For the computation of bilocal contributions for points with two equivalence classes of paths between them (cf. Secs. 3.2 and 4.2) one first needs the appropriate formula for the volume of the intermediate causal interval. Fig. 6.3b illustrates that for $x \in H_y(2)$ the right answer is

$$V(y, x \mid x \in H_y(2)) = 2 \cdot \Delta u\, \Delta v + \Delta u\, (a + b - \Delta v) + \Delta v\, (a + b - \Delta u) = (a + b)\, (\Delta u + \Delta v) \quad (6.11)$$

where $\Delta u = u_x - u_y, \Delta v = v_x - v_y, (a+b) = L/\sqrt{2}$ and one must be aware that the coordinate systems of x and y do not have the same origin. For all 2-path cases we will use these shifted coordinates where the x origin is shifted to the point $(0, L/\sqrt{2}) = (L/\sqrt{2}, 0)$ given in y-coordinates .For the 1-path cases we will keep the former one with coinciding origins.

For points taken from intervals 1 and 8 respectively there are combinations when three different path classes are accessible. Before one tries to find the correct volume formula for that case one should notice that the intermediate volume for two such points will be at least $V(y, x \mid x \in H_y(3)) \geq (a+b)^2$. Thus the integrand for the bilocal contributions will be suppressed with a factor of $\exp(-\rho\, (a + b)^2)$ which makes the integral safely negligible.

Having established this one can start writing down the integrals for all the bilocal contributions on the cylinder. As the different homotopy zones force a further splitting up of the integrals it seems convenient to rethink the earlier introduced artificial splitting up into subintervals to keep things as

simple as possible. $\langle S_{2,n-\text{path}}\rangle(\Omega_i)$ will denote the bilocal contribution to the action expectation value for all $x \in \Omega$ and all $y \in \Omega_i$ where x and y are linked by n different homotopy classes of trajectories. Parity symmetry will be used in Eqns. (6.14) and (6.16) to summarize two identical terms. The split-up of the x-integration in some cases is illustrated in Fig. 6.4a. Furthermore Eq. (6.4) is used to swap the integration order for convenience.

Let us start with all the 1-path contributions for which we can fall back on integrals in Eqns. (6.5,6.8,6.9) by adjusting the boundaries.

$$\begin{aligned}
\langle S_{2,\text{1-path}}\rangle(\Omega_1) &= \int_{\Omega_1} d^2y \int_{\Omega\cap H_y(1)} d^2x\,\rho^2\,p(\rho\,V(y,x \mid x\in H_y(1))) \\
&= \int_0^a du_y \int_0^a dv_y \int_{u_y}^{a+b+u_y} du_x \int_{v_y}^{a+b+v_y} dv_x \rho^2\,p(\rho\,\Delta u\,\Delta v) \\
&= \int_0^a du_y \int_0^a dv_y \left[[\text{integrand } 1]_{\Delta v=0}^{\Delta v=a+b}\right]_{\Delta u=0}^{\Delta u=a+b} \\
&= -\frac{\rho\,a^2}{2}\left(\left(1-\rho\,(a+b)^2\right)\exp(-\rho\,(a+b)^2)-1\right) \qquad (6.12) \\
\langle S_{2,\text{1-path}}\rangle(\Omega_2) &= \int_0^a du_y \int_0^b dv_y \left(\left[[\text{integrand } 1]_{\Delta v=0}^{\Delta v=a+b-v_y}\right]_{\Delta u=0}^{\Delta u=a-u_y}\right. \\
&\quad + \left[[\text{integrand } 1]_{\Delta v=a+b-v_y}^{\Delta v=a+b}\right]_{\Delta u=0}^{\Delta u=a-u_y} \\
&\quad \left. + \left[[\text{integrand } 1]_{\Delta v=0}^{\Delta v=a+b-v_y}\right]_{\Delta u=a-u_y}^{\Delta u=a+b}\right) \\
&= \frac{1}{2}\left(\rho\,a\,b+\exp(-\rho\,a^2)+(-1+\rho\,a^2-\rho\,a\,b)\exp(-\rho\,a\,(a+b))\right. \\
&\quad \left.-\rho\,a\,(a+b)\,\exp(-\rho\,(a+b)^2)\right) \qquad (6.13) \\
\langle S_{2,\text{1-path}}\rangle(\Omega_5) &= \int_0^a du_y \int_0^a dv_y \left(\left[[\text{integrand } 1]_{\Delta v=0}^{\Delta v=a-v_y}\right]_{\Delta u=0}^{\Delta u=a-u_y}\right. \\
&\quad \left. +2\left[[\text{integrand } 1]_{\Delta v=0}^{\Delta v=a-v_y}\right]_{\Delta u=a-u_y}^{\Delta u=a+b}\right) \\
&= \frac{1}{2}\left(1-\exp(-\rho\,a^2)+\rho\,a^2(1-2\exp(-\rho\,a\,(a+b)))\right) \qquad (6.14) \\
\langle S_{2,\text{1-path}}\rangle(\bigcup_{i=4,6,7,8}\Omega_i) &= \int_0^{a+b} du_y \int_0^{a+b} dv_y \left[[\text{integrand } 1]_{\Delta v=0}^{\Delta v=a+b-v_y}\right]_{\Delta u=0}^{\Delta u=a+b-u_y} \\
&= \frac{1}{2}\left(-1+\exp(-\rho\,(a+b)^2)+\rho\,(a+b)^2\right) \qquad (6.15)
\end{aligned}$$

In the high density limit terms with a factor $\exp(-\rho\,(a+b)^2)$ can be neglected. Not generally negligible however are terms with factors $\exp(-\rho\,a^2)$ or $\exp(-\rho\,a\,(a+b))$ as for T only slightly larger than L the value of a will be very small and thus these terms are significant. In the calculations for the 2-path regions the negligible terms will be dropped right away to keep things a little tidier. The 2-path

contributions are:

$$\begin{aligned}
\langle S_{2,2\text{-path}}\rangle(\Omega_1) &= \int_{\Omega_1} d^2y \int_{\Omega\cap H_y(2)} d^2x\,\rho^2\, p(\rho\, V(y,x \mid x\in H_y(2))) \\
&= \int_0^a du_y \int_0^a dv_y \left(\int_{u_y}^a du_x \int_{v_y}^a dv_x \rho^2\, p(\rho\,(a+b)\,(\Delta u+\Delta v)) \right. \\
&\quad \left. +2\cdot \int_{u_y}^a du_x \int_a^{a+b+v_y} dv_x \rho^2\, p(\rho\,(a+b)\,(\Delta u+\Delta v)) \right) \\
&= \int_0^a du_y \int_0^a dv_y \left(\Big[[\text{integrand 2}]_{\Delta v=0}^{\Delta v=a-v_y} \Big]_{\Delta u=0}^{\Delta u=a-u_y} \right. \\
&\quad \left. 2\cdot \Big[[\text{integrand 2}]_{\Delta v=a-v_y}^{\Delta v=a+b} \Big]_{\Delta u=0}^{\Delta u=a-u_y} \right) \\
\text{with} \qquad & \text{integrand 2} = \frac{\rho^2}{2}(\Delta u+\Delta v)^2\, \exp(-\rho\,(a+b)\,(\Delta u+\Delta v)) \\
&= \frac{1}{\rho^2(a+b)^4}\,(-3 \\
&\quad -\exp(-2\rho a(a+b))(3+4\rho ab+4a^2\rho+2\rho^2a^4+4\rho^2a^3b+2\rho^2a^2b^2) \\
&\quad +\exp(-\rho a(a+b))(6+4\rho ab+4\rho a^2+\rho^2a^4+2\rho a^3b+\rho^2a^2b^2)\big) + \text{corr.} \qquad (6.16) \\
\langle S_{2,2\text{-path}}\rangle(\Omega_2) &= \int_0^a du_y \int_0^b dv_y \Big[[\text{integrand 2}]_{\Delta v=0}^{\Delta v=a+b-v_y} \Big]_{\Delta u=0}^{\Delta u=a-u_y} \\
&= \frac{1}{2(a+b)^4\rho^2}\,(-2\rho b(a+b) \\
&\quad +\exp(-\rho a(a+b))(6+\rho(a+b)^2(2-\rho a^2+2\rho ab+\rho(b^2-a^2)a^2)) \\
&\quad -2\exp(-2\rho a(a+b))(3+2\rho a(a+b)(2+\rho a(a+b)))) + \text{corr.} \qquad (6.17) \\
\langle S_{2,2\text{-path}}\rangle(\Omega_5) &= \int_0^a du_y \int_0^a dv_y \Big[[\text{integrand 2}]_{\Delta v=0}^{\Delta v=a-v_y} \Big]_{\Delta u=0}^{\Delta u=a-u_y} \\
&= \frac{1}{(a+b)^4\rho^2}\,(3-2\rho a(a+b) \\
&\quad \exp(-\rho a(a+b))(-6+\rho a(a+b)(-2+\rho a(a+b)(1-\rho a(a+b)))) \\
&\quad \exp(-2\rho a(a+b))(3+2\rho a(a+b)(2+\rho a(a+b)))) + \text{corr.} \qquad (6.18)
\end{aligned}$$

Due to parity symmetry $x \leftrightarrow -x$ one knows $\langle S_2\rangle(\Omega,\Omega_2) = \langle S_2\rangle(\Omega,\Omega_3)$.

Putting together all non-negligible 1-path and the local contributions one has

$$\langle S_{2,1\text{-path,local}}\rangle(\Omega) = \frac{1}{2}\exp(-\rho a^2) - (1+\rho ab)\exp(-\rho a(a+b)) + \text{corr.} \qquad (6.19)$$

The 2-path contributions yield

$$\begin{aligned}
\langle S_{2,2\text{-path}}\rangle(\Omega) &= \frac{-2}{(a+b)^2\rho} + \exp(-\rho a(a+b))\,(1+\rho ab \\
&\quad +\frac{1}{(a+b)^4\rho^2}\,\big((6+2\rho(a+b)(2a+b)-\rho^2(a+b)^2b^2+\rho^3(a+b)^3ab^2) \\
&\quad -2\exp(-\rho a(a+b))(3+4\rho a(a+b)+2\rho^2a^2(a+b)^2)\big) + \text{corr.} \qquad (6.20)
\end{aligned}$$

According to Fig. 6.3a the relation between a, b, T and L is:

$$\begin{aligned}
a &= (T-L)/\sqrt{2} \\
b &= (2L-T)/\sqrt{2} \qquad (6.21)
\end{aligned}$$

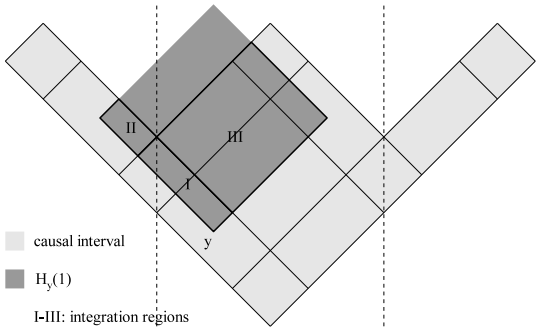

(a) Illustration of the three separate regions for the x integration used in Eq. (6.13). The same has been applied in Eqns. (6.14) and (6.16)

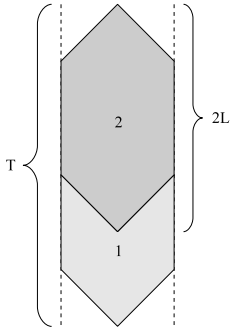

(b) Interval segmentation of the cylinder for $T > 2L$

Figure 6.4: Illustration of integral regions for the cylinder action.

Fig. 6.5a shows a plot of the action and the two contributions. For $T \to 1$ the action approaches the Minkowskian limit $-1/2$. For T only slightly greater than L the exponential corrections to the simple "faces-edges+vertices" rule dominate and cause a spike. For $T \to 2L$ the non-exponential 2-path corrections are all that is left.

For the sake of completeness let us now look at the cylinder with $T > 2L$ and consider a segmentation of Ω according to Fig. 6.4b: For all $y \in \Omega_1$ one has $H_y(1) \subset \Omega$ and $H_y(2) \subset \Omega$. The complete contribution of Ω_2, i.e. $y \in \Omega_2$ and the local contribution of Ω_2 is simply the earlier computed cylinder action for $T = 2L$. So for assembling the complete action one needs to compute

$$\begin{aligned} \langle S_{2,1\text{-path}} \rangle(\Omega, \Omega_1) &= \int_{\Omega_1} d^2y \left[[\text{integrand 1}]_{\Delta v=0}^{\Delta v=L/\sqrt{2}} \right]_{\Delta u=0}^{\Delta u=L/\sqrt{2}} \\ &= (T-2L) \cdot L \cdot \frac{\rho}{2} + \text{corr.} \qquad (6.22) \\ \langle S_{2,2\text{-path}} \rangle(\Omega, \Omega_1) &= \int_{\Omega_1} d^2y \left[[\text{integrand 2}]_{\Delta v=0}^{\Delta v=L/\sqrt{2}} \right]_{\Delta u=0}^{\Delta u=L/\sqrt{2}} \\ &= 0 + \text{corr.} \qquad (6.23) \end{aligned}$$

and the local contribution of Ω_1 which is $-\rho V(\Omega_1)/2 = -\rho(T-2L)L/2$. Up to negligible corrections this cancels with $\langle S_{2,1\text{-path}} \rangle(\Omega, \Omega_1)$. So all that is left is the contribution of Ω_2 for which one can use formulas Eqns. (6.19) and (6.20) where one can now safely neglect all exponentials as $a = a+b = L/\sqrt{2}$. The result is:

$$\langle S \mid \text{cylinder with } T \geq 2L \rangle = \frac{-4}{L^2\rho} \qquad (6.24)$$

In Fig. 6.5b one can see the excellent agreement of the analytic result with simulation data: All features of the data are precisely predicted. For very large ρ one can neglect all 2-path contributions and can fall back to the simple rule of Eq. (6.10) as was done naively at the beginning of this discussion.

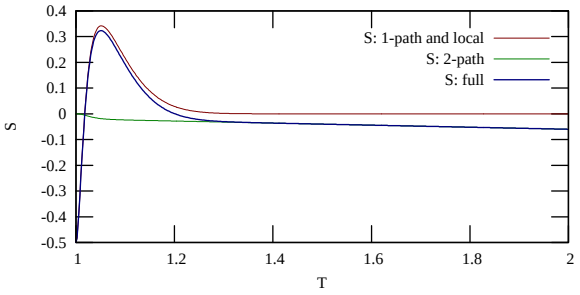

(a) The expected action of a cylinder-interval for $L \leq T \leq 2L$ with $L = 1, \langle N \rangle = 100$: The 2-path contributions and the rest are shown separately.

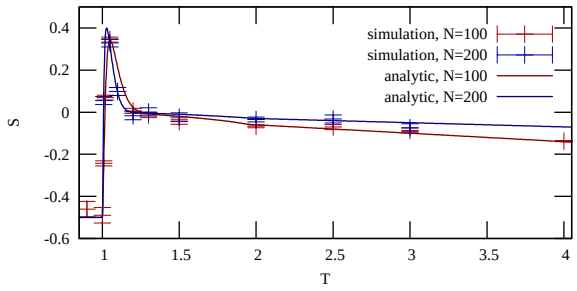

(b) The expected action of a cylinder-interval for $L = 1, \langle N \rangle = 100$ and $\langle N \rangle = 200$ compared with simulation results. For $T \leq L$ one can see the Minkowski-transition.

Figure 6.5: The expected action for causal intervals with height T on the cylinder with circumference $L = 1$

6.4 The Causal Convexity Conjecture

Let us now return to $\mathbb{M}^2$. At the end of Sec. 6.2 it was briefly discussed that causally convex patches of $\mathbb{M}^2$ that are built from causal intervals of finite size all yield $\langle S \rangle = -1/2$ in the high density limit. Consider now a rectangle with edges parallel to the t and x axis. Analytic computation of the expectation value $\langle S \rangle$ is particularly tedious because this type of region is not causally convex: the causal interval of two points near one of the side edges may poke out of the rectangle itself. Therefore averaged simulation data shall be used for the discussion. A sprinkling into a rectangle has three independent parameters that fully characterise the whole setup. A possible choice is the spatial width w, the height along the time-axis h and the sprinkling density ρ.[2] The expectation value $\langle S \rangle$ must be fully determined by these three parameters. The finished causal set has no notion of the original length scale that we were measuring w, h and ρ with. Thus whatever form the function $\langle S \rangle(w, h, \rho)$ might have it must be invariant under rescaling

$$\begin{aligned} w &\to \lambda \cdot w \\ h &\to \lambda \cdot h \\ \rho &\to \lambda^{-2} \cdot \rho. \end{aligned} \tag{6.25}$$

Fig. 6.6 shows simulation data for two different setups with power-law fits. Fig. 6.6a shows $\langle S \rangle$ for constant w and h and varying ρ, Fig. 6.6b for constant w and ρ and for varying h. Given the small relative errorbars the power-law fits look quite convincing and we will assume for now that $\langle S \rangle$ can at least in the regime covered by the simulations be written in the form

$$\langle S \rangle = \text{Const} \cdot h^{\alpha} w^{\beta} \rho^{\gamma}. \tag{6.26}$$

[2] width w, height h and absolute number of expected elements N would be another valid choice that is perfectly equivalent

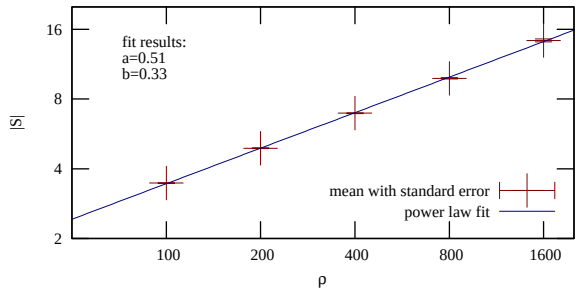

(a) Simulation data for the action of a rectangle in $\mathbb{M}^2$ for $w = h = 1$, varying density ρ with a power-law fit. Data averaged over 10^6 to 10^7 runs. Fit function: $\rho^a \cdot b$.

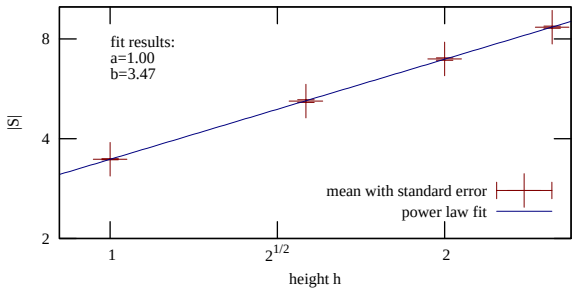

(b) Simulation data for the action of a rectangle in $\mathbb{M}^2$ for $w = 1, \rho = 100$, varying height h with a power-law fit. Data averaged over 10^6 to 10^7 runs. Fit function: $h^a \cdot b$.

Figure 6.6: Numerical results for the action of a rectangle in $\mathbb{M}^2$.

The aforementioned scale invariance (cf. Eq. (6.25)) demands $\alpha + \beta - 2\gamma = 0$. From simulation 1 (Fig. 6.6a) one is tempted to deduce $\gamma = 1/2$ and from simulation 2 (Fig. 6.6b) that $\alpha = 1$. It follows $\beta = 0$.

The fact that for constant ρ the width does not affect the value of the action whereas $\langle S \rangle \propto h$ supports the assumption that only elements that are near the spatial borders, but not elements in the bulk of the area, far away from these borders, do contribute to the action. At the same time for large density the bilocal contributions where both elements are near the spatial borders are the only ones that are affected by the causal non-convexity of the sprinkling region. Thus it is tempting to suppose that causal non-convexity causes the unbounded growth of the action whereas for convex causal intervals and constructions made thereof it is always $-1/2$. In fact one might go so far as to conjecture that on $\mathbb{M}^2$ the expected action of any causally convex region is $-1/2$. To this date there is no proof for this conjecture but as far as the author is aware there is also no counter-example yet.

6.5 Fluctuations Of The Action

At the beginning of this chapter the action was introduced as a potential tool to identify manifold like causal sets and the mean of the action has been investigated on certain manifold patches. However when it comes to deciding whether a single given causal set is similar to some kind of manifold, not only the mean but also the closeness of a single evaluation to that mean is important. In short: One must investigate the fluctuations of the action.

Recalling Eq. (6.2) the action is the sum of the local discrete d'Alembertian, without the prefactor $4 \cdot l^{-2}$, over every point of the set. As was pointed out, the fluctuations of the local d'Alembertian grow with the number of set elements. So for the summed up action there are two potential effects: If the correlations of the d'Alembertian evaluated at different points are small then it should approximately hold

$$\sigma_S = \sqrt{N}\, \sigma_{B'}$$

where B' denotes the d'Alembertian without the prefactor and σ_X denotes the fluctuations of the quantity X. An estimate shows that the fluctuations of B' should asymptotically scale like $\sqrt{\log(N)}$ for large N.[3] So for weak correlations the action fluctuations should scale at least like $\sqrt{N}$ and thus the action in the introduced form is unlikely to be a suitable measure for manifold-likeness.

But it could also be possible that there are strong anti-correlations between the d'Alembertians of neighbouring points which lead to a smoothing effect and make the action a more well behaved quantity.

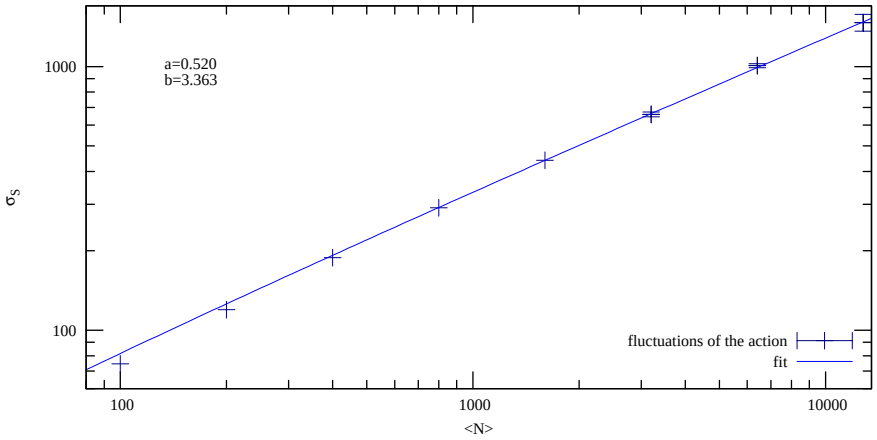

Figure 6.7: Fluctuations of the action of a causal interval in $\mathbb{M}^2$ with a fit to $\sigma_S(\langle N\rangle) = b \cdot (\langle N\rangle \log\langle N\rangle)^a$.

Unfortunately numerical simulations indicate that the fluctuations grow with N as shown in Fig. 6.7. The fit is not very good but it is clear that the action grows roughly like $\sqrt{\langle N\rangle}$ and thus there seems to be no hope for a damping induced by anti-correlations. Of course this is only an assumption based on the numerical data that is available which can not give a comprehensive picture of what is going on. Still it seems reasonable to think about alternatives to the currently proposed action. A potential enhancement could be using the non-local d'Alembertian to damp fluctuations. However we have seen in Chapter 5 that the introduction of the intermediate length scale also introduces new correction terms so the consequences of this step must be carefully investigated.

6.6 The Action And Curvature

Earlier in this chapter hints that the action might be a topological invariant have been mentioned. So we naturally have to study how it reacts to the presence of curvature. Again we will use two dimensional de Sitter space as a simple object of study. Unfortunately here both the analytical and numerical approach are very challenging: The integrals for the expectation value are made harder by the conformal factor of the metric that significantly complicates the volume formula. Numerical

[3] This was revealed to the author in private communication with Fay Dowker.

simulations however require enormous computational effort for large causal sets. As one needs to analyse the cardinality of all possible causal intervals in the set the number of necessary computation steps roughly scales like $\mathcal{O}(N^3)$. At the same time as has been indicated in the last section the standard deviation of the outcome grows so that for higher N more and more runs become necessary to obtain the same standard error. The datapoint in Fig. 6.8b for $\langle N \rangle = 4000$ took up more than two weeks of CPU time and still has an enormous standard error. This illustrates how hard it is here even by simulations to gain a comprehensive insight. A third option to tackle the problem would be numerical integration. But as shown in Fig. 5.2c multidimensional numerical integration of volatile functions can lead to instabilities and it is hard to rule out such problems. So for now the only hints available are shown in Fig. 6.8.

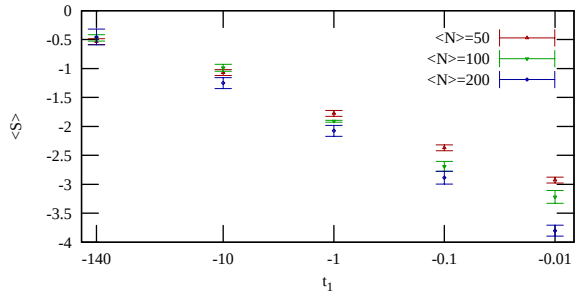

(a) Expected action for various interval sizes and element numbers

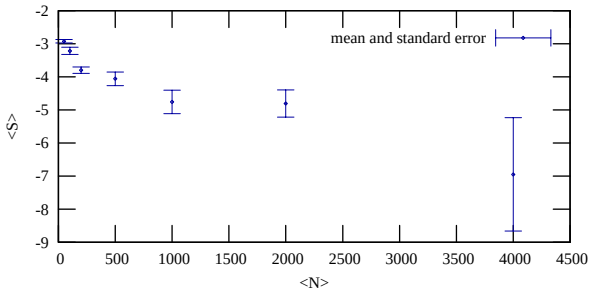

(b) Expected action for $t_1 = -0.01$ fixed and various element numbers.

Figure 6.8: Numerical results for the expected action $\langle S \rangle$ on de Sitter 2d for causal intervals between $(t_0, 0)$ and $(t_1, 0)$ for $t_0 = -150$ and varying t_1 and expected number of elements $\langle N \rangle$. Averaged data from 2E4 to 5E5 runs.

Fig. 6.8a shows how the action behaves when one increases the size of the interval. For very small sizes one can see the Minkowskian limit which is in agreement to the observations in chapter 5: The action is approximately $-1/2$ regardless of the element number. For bigger interval sizes the action tends towards smaller values, away from $-1/2$. This is clearly not what one expects from a topological invariant. Furthermore the actions for different densities deviate: The larger the density the larger will be the absolute value of the action. Unfortunately considering the data shown in Fig. 6.8b it is impossible to judge whether it tends towards a finite value or whether it will diverge for $\langle N \rangle \to \infty$.

On $\mathbb{M}^2$ the average d'Alembertian of $\phi = 1$ is zero. When summing up the action the only contributions come from regions near the boundary where the cut-off disturbs the d'Alembertian. On de Sitter the bulk d'Alembertian contributions are not zero but $-R/2 = -1$. Taking into account the intrinsic cut-off of the de Sitter 2d geometry (cf. Sec. 5.3) one expects a term scaling roughly like $-N$ from the inner part of the sprinkling for large enough intervals. At the same time the boundary terms may also grow and it is hard to tell without precise calculations what the total action will look like. The regime in which the d'Alembertian correctly tends towards $-R/2$ requires $l_p \ll l_c \lesssim l_v$ which

again requires a high enough sprinkling density and which therefore is numerically hard to investigate. So the question whether the bulk or the boundary terms dominate in the high density limit cannot be answered here. It is however crucial for the potential application of the action. Curvature is an essential phenomenon of realistic theories. So an action must be able to deal with it.

Chapter 7

A Roadmap For Causal Set Theory

We have now seen approaches to recover information about curvature and topology from a causal set. These are concepts known from continuum geometry. Furthermore we have discussed discrete equivalents of retarded propagators and the d'Alembert operator, two vital components of the language of partial differential equations. In the last chapter a proposed action to find manifold-like causal sets has been introduced. All this is part of establishing the relation between manifolds and causal sets. So it more or less serves the purpose of translating concepts that we know to the new spacetime description.

But causal set theory was intended to be more than a mere new language. People who are working with it are convinced that the notion of discrete atomic elements that are ordered by causality is actually true. So eventually causal set theory must supply more: It must describe how the net that forms spacetime is created. The proposed action is in fact a first step in that direction: In [14] it is discussed that the action might not just be useful to find arbitrary manifold-like causal sets but such sets that are equivalent to manifolds that satisfy Einstein's equations. These equations give a description of the interaction of matter and spacetime which is another thing that causal set theory must eventually be able to provide.

So there is still more than enough work to be done. In the end one thing matters in particular for a physical theory: Is it able to make predictions about the observable reality? Physicists must try to deduce how the discreteness of space might be detectable by experiment. This is very hard as the discreteness scale is conjectured to be so very small. Therefore people try to derive new phenomenology with a lot of creativity. But one must always keep in mind: It must not just be a new prediction. Most importantly it must be true.

Appendix A

Documentation Of *Koko*

A.1 Prerequisites

Koko is a causal set code suite for `C++` that was written to perform the simulations required for the research this thesis is about.[1] As these simulations are a crucial part of the thesis and because other causal set researchers might benefit from reusing the code it shall be documented here.

Koko is available under the GNU General Public License Version 3. So anyone is welcome to modify it and to work with it as long as he or she only redistributes it under the latest GNU GPL. The full information on the license can be found in the read-me that comes with the package.

In order to work with the code it will be necessary to work directly with `C++`. So one needs a working way of editing and compiling code files (e.g. one of many available IDEs) and a certain level of understanding of the language: The very basic elements of `C++` like atomic data types, functions, classes, handling console applications and file output. More elaborate language elements that are used are the vector template, class inheritance and pointers.

The code is set up as a console application and should run under any operating system. However, depending on your environment some basic functions like `round(),sqr()` or `min()` or the constant `M_PI` might either already be defined or must be defined manually in the file "`Common/Tools.h`".

A.2 Concept And Basic Functionality

The basic functionality that *Koko* supplies is a framework to describe the desired sprinkling region, create sprinklings therein and to compute the adjacency matrices of the causet. To this end there are four major interacting classes: `Tp`, `TGeometry` (both defined in "`Common/UnitGeometry.h`"), `TSprinkling` ("`Common/UnitSprinkling.h`") and `TConnection` ("`Common/UnitConnection.h`"). Their properties and important methods are briefly listed in the Tables A.1, A.2 and A.3. The classes `Tp` and `TGeometry` as presented in Table A.1 do not describe an actual spacetime region of interest but are

[1] *Koko* stands for *cau*sal set *co*de.

Class `Tp`	
	Stores the coordinates of a single sprinkled point on the manifold.
`double t`	
	Stores the time coordinate of the point.

Class `TGeometry`	
	Describes the necessary properties of the spacetime region the sprinkling shall be performed in.
`double V`	
	Stores the volume of the spacetime region.
`TGeometry()`	
	Constructor: Initializes the instance.
`virtual Tp *getRandomPoint()`	
	Returns a pointer to a newly created instance of `Tp` that holds the coordinates of a randomly picked sprinkling point.
`virtual bool isCausal(Tp *a, Tp *b)`	
	Returns `true` if the point referred to by `a` is to the causal past of the point referred to by `b` on the spacetime. Otherwise it returns `false`.
`virtual int countCausal(Tp *a, Tp *b)`	
	Returns the number of equivalence classes of causal trajectories from the point referred to by `a` to the point referred to by `b`.

Table A.1: Overview of the `Tp` and `TGeometry` class

merely dummies defined to supply at least formally the minimal requirements for the interaction with the `TSprinkling` class. To describe a real scenario one might want to alter these definitions: Add additional coordinates in `Tp` and fill the methods of `TGeometry` with useful instructions. However there is a much more elegant way. For performing sprinklings into actual spacetimes define two new classes. One derived from `Tp` and one derived from `TGeometry`. The sub class of `Tp` must have additional `double` variables to store the rest of the coordinates. In the sub class of `TGeometry` the constructor must initialize `V` with the correct volume of the sprinkling region. `getRandomPoint()` must supply correctly distributed points and `isCausal()` and `countCausal()` must return appropriate answers for the manifold one wants to sprinkle in. Examples of how this could be done are given in the files "`Common/UnitGeometry_Minkowski2d.h`", "`Common/UnitGeometry_deSitter2d.h`" and "`Common/UnitGeometry_Cylinder2d.h`" that define sub classes to perform sprinklings into the respective spacetimes. By the concept of inheritance the `TSprinkling` class will also work when called with a pointer to the new geometry sub class. As all methods in the original `TGeometry` class were declared to be `virtual` they will be overridden by the meaningful new methods supplied by the sub

Class `TSprinkling`	
	Creates and handles the list of sprinkling elements by using a given instance of `TGeometry`.
`vector<Tp*> vertex`	
	This list stores the set of sprinkled points.
`TGeometry *geometry`	
	Stores a pointer to the instance of `TGeometry` that is used for performing the sprinkling.
`int size`	
	Stores the number of sprinkled elements.
`TSprinkling(int count_exp, TGeometry *_geometry)`	
	This will create a sprinkling with `count_exp` expected number of elements onto the spacetime region described by the instance referred to by `geometry` which will be set to `_geometry`. `count_exp` is assumed to be big enough so that the Poisson distribution is well approximated by a Gaussian distribution. Hence the actual number of elements is picked via a Gaussian with mean `count_exp` and width $\sqrt{\texttt{count\_exp}}$.
`TSprinkling(int count_exp, bool randomCount, TGeometry *_geometry)`	
	The same constructor but by calling with `randomCount=false` the number of sprinkling elements will be precisely `count_exp`.
`~TSprinkling()`	
	The destructor deletes the set of points referred to by the entries of `vertex`.
`void addRandom(int count)`	
	This method will add `count` points to the sprinkling by calling the method `getRandomPoint()` of the instance of `TGeometry` that `geometry` refers to.
`bool isCausal(int i, int j)`	
	The concept of *Koko* is that "above" `TSprinkling` there should be no direct interaction with any `TGeometry` instances any more. This method passes the question whether the point referred to by `vertex[i]` is to the causal past of the point referred to by `vertex[j]` on to the instance of `TGeometry` that `geometry` refers to.
`void sort()`	
	In its current form *Koko* assumes that for all spacetime regions in question there is a global coordinate `t` whose gradient is always timelike so that a point `a` can only be to the past of `b` if `a.t<b.t`. Thus after creating the list `vertex` of points `TSprinkling` will sort them by `t` in ascending order by calling this method. Thus after sorting one can immediately tell that `vertex[i]` can only be to the past of `vertex[j]` if `i<j`.

Table A.2: Overview of the `TSprinkling` class

Class `TConnection`	
	Creates and handles the adjacency matrices A_C and A_R from a given instance of `TSprinkling`. Within `TConnection` a causet element will only be referred to by an integer that is determined by the position of that element in the list `vertex` of the given instance of `TSprinkling`.
`vector< vector<bool> > storeCausal,storeLink`	
	These two dimensional lists store the entries of the adjacency matrices. `storeCausal` will contain the data for A_C and `storeLink` the data for A_R.
`int size`	
	The number of sprinkling elements.
`TConnection(TSprinkling *Sprinkling)`	
	Constructor: Initializes causal and link data. `size` is set to `Sprinkling->size`, `createCausalFromSprinkling(Sprinkling)` and `createLinkTable()` are called.
`TConnection(TSprinkling *Sprinkling, bool needLinks)`	
	If called with `needLinks=false` no link matrix will be created.
`void createCausalFromSprinkling(TSprinkling *Sprinkling)`	
	This method initializes `causalStorage` using the instance of `TSprinkling` referred to by `Sprinkling`. The list `Sprinkling->vertex` is assumed to be sorted by `t`. This means A_C is upper triangular. Thus not the full square matrix is stored in `causalStorage` but only the upper triangle. `storageCausal` has size `size` and `storageCausal[i]` has size `size-i-1`. `storageCausal[i][j]` stores the result of `Sprinkling->isCausal(i,i+j+1)`.
`bool causal(int i, int j)`	
	For most applications it is convenient to be able to work with the full causal matrix. This translates between the full matrix and the storage of the upper triangle data in `storageCausal`: The method returns true if `storageCausal[i][j-i-1]=true` otherwise `false`.
`void createLinkTable()`	
	After the initialization of `storageCausal` this initializes `storageLink` which is organized in exactly the same way.
`bool link(int i, int j)`	
	This is the link-equivalent of the `causal` method.
`vector<bool> getInterval(int i, int j)`	
	This method returns a `vector<bool>` of size `size` where entry `k` is true iff `causal(i,k)=causal(k,j)=true`.
`int getCardinality(int i, int j)`	
	Returns the number of elements `k` such that `causal(i,k)` and `causal(k,j)` is true.

Table A.3: Overview of the `TConnection` class

class.

For clarity the de Sitter 2d example shall briefly be discussed here. We will use conformally flat coordinates (cf. Sec. 2.4.4). The sprinkling region of interest is a causal interval between the points $(t_0, 0)$ and $(t_1, 0)$. The sub classes `Tp_deSitter2d` and `TGeometry_deSitter2d` are defined based on the classes `Tp` and `TGeometry`. In `Tp_deSitter2d` an additional coordinate `double x` is defined to hold the spatial position of each point. In `TGeometry_deSitter2d` the constructor takes the arguments `alpha`, `t0` and `t1` that determine the metric scale factor and the coordinates of the start and end point of the interval. The method `getRandomPoint()` sprinkles points into a rectangle $[t_0, t_1] \times [-(t_1 - t_0)/2, (t_1 - t_0)/2]$ according to Eq. (2.20) and rejects the points until one inside the interval is found. A pointer to that point is then returned. Due to conformal flatness the lightcones in these coordinates are just like in $\mathbb{M}^2$ which is why the physical part of the implementation of the `isCausal()` method is straightforward. Note however that the method is via inheritance required to accept pointers to the fundamental `Tp` class whereas inside it needs to work with instances of `Tp_deSitter2d`. Therefore the two pointers must be typecast before their de Sitter-specific `x` variable can be accessed. As between any two pairs of points there is at most one equivalent class of paths the function `countCausal()` only needs to return 1 if `isCausal()` returns `true` and 0 else. Therefore the original method defined in `TGeometry` is totally sufficient and no new version needs to be defined in the sub class.

A.3 Examples And Application

Koko comes with some simple examples of how to use that fundamental causet handling functionality to built more complex applications.

The algorithm introduced in Chapter 4 that approximately recovers the homotopy zones of a point is implemented in "`Common/UnitHomotopyAlgorithm.h`" and an application that uses it is given in "`Examples/HomotopyAlgorithm.cpp`".

A class to compute the discrete d'Alembertian as introduced in Chapter 5 is defined in "`Common/UnitDAlembertian.h`" and "`Examples/DiscreteDAlembertian.cpp`" gives basic examples of how to use that class and of how to collect the layer cardinality data $\langle N_{\mathrm{card}}(x, n) \rangle$.

In "`Examples/Action.cpp`" an application that computes the action defined in Chapter 6 is given.

Bibliography

[1] S. Major, D. Rideout, and S. Surya, "On recovering continuum topology from a causal set," *J.Math.Phys.*, vol. 48, p. 032501, 2007, arXiv:gr-qc/0604124v3.

[2] S. W. Hawking, A. R. King, and P. J. McCarthy, "A new topology for curved space-time which incorporates the causal, differential, and conformal structures," *J. Math. Phys.*, vol. 17, pp. 174–181, 1976.

[3] D. B. Malament, "The class of continuous timelike curves determines the topology of spacetime," *J. Math. Phys.*, vol. 18, pp. 1399–1404, 1977.

[4] A. V. Levichev, "Prescribing the conformal geometry of a lorentz manifold by means of its causal structure," *Soviet Math. Dokl.*, vol. 35, pp. 452–455, 1987.

[5] D. P. Rideout and R. D. Sorkin, "A classical sequential growth dynamics for causal sets," *Phys.Rev.D*, vol. 61, p. 024002, 2000, arXiv:gr-qc/9904062v3.

[6] M. Ahmed and D. Rideout, "Indications of de sitter spacetime from classical sequential growth dynamics of causal sets," *Phys.Rev.D*, vol. 81, p. 083528, 2010, arXiv:0909.4771v2.

[7] N. D. Birrell and P. Davies, *Quantum fields in curved space*. Cambridge University Press, 1982.

[8] S. Johnston, "Feynman propagator for a free scalar field on a causal set," *Phys.Rev.Lett.*, vol. 103, p. 180401, 2009, arXiv:0909.0944v2.

[9] S. Johnston, "Particle propagators on discrete spacetime," *Class.Quant.Grav.*, vol. 25, p. 202001, 2008, arXiv:0806.3083v2.

[10] R. Brown, *Elements of Modern Topology*. McGraw-Hill, 1968.

[11] E. Poisson, "The motion of point particles in curved spacetime," *Living Reviews in Relativity*, vol. 7, no. 6, 2004, http://www.livingreviews.org/lrr-2004-6 cited on 09/09/2010.

[12] G. W. Gibbons and S. N. Solodukhin, "The geometry of small causal diamonds," *Phys.Lett.B*, vol. 649, pp. 317–324, 2007, arXiv:hep-th/0703098v2.

[13] R. D. Sorkin, "Does locality fail at intermediate length-scales," in *Approaches to Quantum Gravity* (D. Oriti, ed.), Cambridge University Press, 2009, arXiv:gr-qc/0703099.

[14] D. M. Benincasa and F. Dowker, "The scalar curvature of a causal set," *Phys.Rev.Lett.*, vol. 104, p. 181301, 2010, arXiv:1001.2725.

[15] D. J. Kleitman and B. L. Rothschild, "Asymptotic enumeration of partial orders on a finite set," *Trans. Amer. Math. Soc.*, vol. 205, pp. 205–220, 1975.